OBSERVATIONS OF ELF NOISE BANDS WITH SATELLITE INJUN III

by

Thomas B. Burns

A thesis submitted in partial fulfillment of the
requirements for the degree of Master of Science in the
Department of Physics and Astronomy
in the Graduate College of
The University of Iowa

June 1967

Thesis supervisor: Assistant Professor Donald A. Gurnett

Graduate College
The University of Iowa
Iowa City, Iowa

CERTIFICATE OF APPROVAL

MASTER'S THESIS

This is to certify that the Master's Thesis of

THOMAS B. BURNS

with a major in Physics has been approved by the Examining Committee as satisfactory for the thesis requirement for the Master of Science degree at the convocation of June 9, 1967

Thesis committee: _____
Thesis supervisor

_____
Member

_____
Member

ACKNOWLEDGMENTS

I wish to thank Dr. Donald Gurnett for suggesting this research project and express my sincere appreciation for his help, interest and encouragement. I also wish to acknowledge many useful and interesting discussions with Dr. Stanley Shawhan and thank him for his interest and help. Without the help of the above, this thesis could never have been written.

Thanks are also due Mr. Mark Baumbach and Mr. Robert Shaw for their help with the graphs and for their production of the Missilyzer spectrograms. Mrs. Dora Walker is to be especially thanked for her efficient and reliable operation of the Spectran analysis equipment. I am also indebted to Mr. Roger Anderson and Mr. William Taylor for many forms of assistance.

It is pleasant to be able to acknowledge Mrs. Ida McClain for her excellent typing of this manuscript, and Mr. Dave Lunde who cheerfully persevered through the drafting of many of the figures. I am also glad to acknowledge the help I received from the entire group of people in Satellite Analysis.

This work was supported in part by the Office of Naval Research under contract Nonr 1509(06) and in part by the National Aeronautics and Space Administration under grant NGR 16-001 043.

ABSTRACT

The most common type of VLF emission received by the Injun III satellite was ELF hiss, whose spectral shape remains approximately constant and which has frequency components below 1.5 kHz, and chorus, which is a sequence of discrete emissions. When ELF hiss has a sharp low frequency cutoff (F_c), we call it an ELF noise band. In this thesis, we present a study of the ELF noise bands found in the Injun III VLF data.

An investigation of the characteristics of ELF noise bands shows that chorus is present on nearly every pass for which an ELF noise band occurs. Because of the presence of chorus an upper frequency cutoff is difficult to observe.

The region of maximum probability of occurrence for ELF noise bands is found to be in the interval $6 \leq \text{MLT} < 11$ and $50° \leq \text{INV} < 70°$. Factors which may have caused the experimental percentages to be lower than actual percentages are discussed.

By plotting the variation of F_c with altitude we can see below what frequency radiation was not received by the satellite at a given altitude. Choosing the proton gyrofrequency as a normalizing factor for F_c we find that most experimental points are less than and within 10% of the proton gyrofrequency for all altitudes, although we find increased scatter at higher latitudes. An investigation of

three individual passes allows us to study the variation of F_c with the orbital parameters of the satellite.

Although the cutoff can be either a propagation effect or a source effect, we compare only the predictions of a propagation effect. The propagation effect is the cutoff of left-hand circularly polarized waves at frequencies below the proton gyrofrequency. Assuming a midlatitude model ionosphere we find agreement at the lowest latitudes, but at higher latitudes, F_c for a given altitude is generally smaller than the cutoff predicted by our model.

TABLE OF CONTENTS

1. INTRODUCTION

Electromagnetic radiation with frequency components between 1 kHz and 30 kHz is usually defined as being in the VLF (Very Low Frequency) region. For purposes of this study, we shall call naturally occurring electromagnetic radiation with frequency components from 100 Hz to 1500 Hz, ELF (Extremely Low Frequency) noises.

Noises in the VLF and ELF regions were classified by Gallet [1959] into two large groups. The first group contains whistlers, which are caused by lightning discharges. All frequencies are emitted simultaneously by the lightning discharge, and the spectral shape of the whistler is due to dispersion along the path.

In the second group are VLF emissions, which are not caused by lightning discharges, but which are believed to be generated by instabilities in the magnetosphere. There are two principal types of VLF emissions. The first type is continuous in time and frequency (steady-state situation) and the second type is discrete, but may have a strong repetition tendency (transient-state situation).

Hiss is an incoherent, band-limited, white noise with a duration of minutes and with little temporal structure on a time scale less than one second [Helliwell, 1965]. Hiss thus belongs to the first category of VLF emissions. An example of ELF hiss is shown in Figure 1. For this study, we define ELF noise bands as ELF hiss with a sharp low frequency cutoff.

Chorus is a sequence, lasting on the order of seconds, of discrete emissions [Helliwell, 1965]. This emission belongs to the second category, and an example of it is shown in Figure 2. Chorus is sometimes classified into two subgroups:

(1) Chorus with a frequency range of 2-4 kHz. Storey [1953] called this noise "dawn chorus" and found it to have a maximum occurrence at about 0600 local time. Allcock [1957] and pope [1957] found that the time of maximum occurrence increases with the geomagnetic latitude of the receiving station.

(2) Chorus with a frequency range below 1.5 kHz. This type of chorus is often called "roar" [Brice, 1964], or "polar chorus" [Ungstrup and Jackerott, 1963]. Chorus in this frequency range has been reported for stations with high geomagnetic latitudes such as Godhaven, Greenland (79.9°) [Ungstrup, 1959], College, Alaska (64.7°N) [Pope, 1959], Kiruna, Sweden (65.3°N) [Aarons et al., 1960] and Bryd Station, Antartica (70.5°S) [Helliwell et al., 1962]. Ungstrup and Jackerott [1963] found that the frequency of occurrence has a maximum at a local mean time of 0901, and also found a negative correlation coefficient between the number of hours with polar chorus per day and the daily sum of the local K_p index at Godhaven.

Satellites which have carried experiments for observing VLF noises include: Vanguard III, Injun III, Alouette I, Alouette II, Lofti I, Lofti IIA, OGO I, II and III. In Section 2, we describe

the Injun III VLF experiment and summarize some findings which are related to this study.

Considerable processing is involved in the reduction of the raw data from the Injun III VLF experiment to measurable physical quantities, such as low frequency cutoffs. The data analysis procedure and possible factors which may cause the data to be misinterpreted are discussed in Section 3. In Section 4 the characteristics of ELF noise bands are discussed.

In order to make comparisons of the VLF data of Injun III with ground observations of VLF noise, results from a study of the density of occurrence in satellite data are given in Section 5. As a measure of local time, we shall use Magnetic Local Time (MLT), which is defined as the hour angle between the magnetic meridian through the satellite and the magnetic meridian through the sun, using the centered dipole approximation [Chamberlain, 1961]. For latitude, we shall use invariant latitude, which is defined by the relation INV = arccos $(L^{-1/2})$, where L is the shell parameter of McIlwain [1962]. The variations of the low frequency cutoff (F_c) and the ratio (A) of F_c to the proton gyrofrequency (Ω_p), with respect to altitude, are also discussed in Section 5.

In Section 6, a somewhat detailed investigation is made of three individual passes of the satellite. For these passes the variation of F_c is studied with respect to all orbital parameters of the satellite. Combining the results of the statistical study and

the individual pass study, possible explanations of the cutoff of the ELF noise bands are discussed in Section 7.

2. DESCRIPTION OF THE INJUN III VLF EXPERIMENT AND SUMMARY OF PREVIOUS INJUN III RESULTS ON ELF NOISE

A primary objective of the Injun III satellite was the study of VLF phenomena and its possible correlation with the properties of the natural and artificial radiation zones, auroras and airglow. On this satellite, a magnetic loop antenna was used to detect the magnetic component of VLF radiation in the range of 0.1 to 7.2 kHz.

To provide maximum coupling between the antenna and a wave propagating in the longitudinal mode (such as a whistler), the satellite was oriented so that the geomagnetic field vector was in the plane of the loop antenna. The signal from the preamplifier was normalized by an Automatic Gain Control (AGC) to a constant output amplitude which modulated the telemetry transmission at 136.86 MHz.

There were three measurements made by the Injun III VLF experiment:

(1) The spectrum analyzer measured the absolute amplitude of the noise spectrum at 0.7, 2.7, 4.3, 5.5, 7.0 and 8.8 kHz. The spectrum analyzer did not respond to noise bursts with a time constant less than 0.1 sec.

(2) The AGC feedback voltage measured the rms magnetic field strength in the 0.1 to 7.2 kHz range.

(3) A high time resolution frequency-time spectrum was obtained from the wide band VLF signal telemetered to the ground. Figure 3 shows the frequency response of the wide band VLF system on Injun III.

The Injun III VLF experiment is described in detail by Gurnett [1963] and by Gurnett and O'Brien [1964]. A complete discussion of the Injun III satellite and a description of all its experiments is given by O'Brien, Laughlin and Gurnett [1962].

In the interpretation of data from Injun III, the assumption must be made that the satellite did not disturb the medium enough to cause VLF noise or to affect the absolute amplitude measurements. For many of the VLF noises observed, this assumption has been supported by the similarity of the spectral character of VLF emissions observed by Injun III with ground receivers [Gurnett, 1963]. The statistical occurrence of satellite ELF and VLF noise and their comparison with that from ground based receivers may be considered further evidence in support of this assumption.

ELF hiss bands, having frequency components as low as 200 Hz, were also reported by Gurnett [1963]. These hiss bands were often found to have an upper frequency limit. Hiss with frequencies less than 1 kHz and chorus were the most common VLF noises observed at the satellite. These strong noises can be considered to have caused the frequent saturation of the 0.7 kHz channel.

Preliminary observations of noise bands such as those shown in Figure 4 were reported by Gurnett [1965]. These noise bands

were characterized by the VLF noise occurring at about 1 kHz having a frequency cutoff near the proton gyrofrequency. Below Ω_p, another noise band can be seen with a frequency cutoff near the He^+ gyrofrequency (Ω_2). It can also be seen that the upper cutoff frequency components of these noise bands are composed of chorus emissions.

These noise bands are unusual in that more than one cutoff is readily observed. We should mention that both of these events occurred when the satellite was at low altitudes and high latitudes. Also the perigee of the satellite was in the northern hemisphere at this time (see Figure 5). It will be shown in Section 4 that this combination of factors would cause these noise bands to be rarely found.

3. DATA ANALYSIS

The VLF data received by Injun III was telemetered on command to the ground tracking stations. There it was recorded on magnetic tape. At most stations, the WWV time signal and either a 10 kHz or a 4.096 kHz reference tone were recorded on other channels. The tapes were then sent to the University of Iowa for analysis.

In the processing of the Injun III VLF data, four instruments are relied on for much of the data analysis. These instruments are:

(1) The Spectran series 480 Real Time Spectrum Analyzer (model 480-25);

(2) A digital clock;

(3) The Benson-Lehner Oscar/Digital Decimal Model F System;

(4) The Kay Electric "Missilyzer" Audio and Sub-audio Sonograph.

The use of these instruments is discussed below:

(1) The Spectran gives high resolution analysis by using 480 high Q Magnetorestrictive rod filters of transient and steady state signals in a bandwidth of 10 kHz for tapes run at real time speed. The use of 480 filters sets a best accuracy of 20 Hz for the 10 kHz range. The output of each filter is selected by a

capacitive commutator, which also provides a synchronized frequency sweep signal for an oscilloscope. The amplitude of the signal from each filter modulates the intensity of the oscilloscope beam.

A spectrogram is produced by taking a moving film picture of the oscilloscope screen. The relative intensity of any frequency component is represented by a darkening of the film.

In order to calibrate the Spectran, a square wave signal of known frequency, say 1.0 kHz or 200 Hz is fed through it. Filters sampling at multiples of this frequency will become excited and a series of dots will appear on the oscilloscope screen. For a spectrogram with a frequency range of 0-1.6 kHz, these dots are about 25 Hz wide. This limits the accuracy of any measurement. From inspection of Figures 1 and 2, we can see that the calibration is nearly linear for about only two-thirds of the frequency range. The non-linearity of the calibration did not affect the accuracy of measurements as much as the width of the calibration dots.

(2) The digital clock is driven by the reference tone (either 10 kHz or 4.096 kHz). This clock generates the calibration markings, and displays them for two seconds every minute on the oscilloscope screen. The calibration is nearly linear up to approximately 6 kHz for tapes run at real time speed.

(3) The "Oscar" has a projection system which can enlarge a 70 mm x 35 mm section of film into a 60 cm x 30 cm image projected

on a ground glass screen. Two hairlines can be moved across the screen for purposes of calibration and measurement. Using the "Oscar", the measurement procedure converts information on the film into digital form punched out on IBM cards. On the same card as this information, identifying data, such as the time of the event, are usually punched.

(4) The Missilyzer can be used in any of four frequency ranges (5-500 Hz, 15-1500 Hz, 50-5000 Hz and 150-15,000 Hz). Two different methods of analysis of VLF data are possible using the Missilyzer. The first method of analysis relates frequency and amplitude to time; the second method relates amplitude to frequency at a given instant of time. For the first method, the amplitude is given by the relative darkening of the paper; while for the second method (called sectioning) a picture of signal amplitude along the horizontal plane versus frequency along the vertical plane is given. It is possible, by halving the frequency range used, to put both types of Missilyzer analysis on the same recording paper. When this is done, the frequency scale on the Section is inverted. We can also halve the frequency range by using an expanded scale. For this study, the 50-5000 Hz range was used on the expanded scale. Figures 6 to 12 contain examples of Missilyzer-sectionings. The disadvantage in using the Missilyzer is that the production of a Missilyzer-sectioning takes over five

minutes. For this study, Missilyzer-sectionings were generally used only for verifications of frequency spectra of ELF noise bands found on Spectran spectrograms.

In order to make measurements on low frequency cutoffs of ELF noise bands, tapes were run through the Spectran at 4 times the normal speed. When the tapes were run through the Spectran at this speed, spectrograms with a frequency range of 0-1.6 kHz could be produced. These spectrograms had a frequency scale which was $\pm$ 5% linear up to about 1.2 kHz.

In order to determine how accurately a frequency could be measured with the "Spectran-Oscar" system, the frequency of interference tones at 472 Hz were measured. Comparison of the measured values with the actual value showed that there was an rms error of ~ 25 Hz between the two values. Thus measurements of F_c were made to an accuracy of 25 Hz.

Another factor which could affect the measurement of low frequency cutoffs is the fall-off in response of the wideband VLF receiver. However this factor would be important only if the Spectran had a flat frequency response. By making a spectrogram of a "white noise" signal, it was found that filters in the range of 355 Hz (for 0-1.6 spectrograms) had weak responses. With the measurement error taken into consideration, 380 Hz was taken as the lower limit for F_c.

4. CHARACTERISTICS OF SATELLITE ELF NOISE BANDS

In order to determine whether ELF noise bands were present on a given pass of Injun III, spectrograms in the 0-8 kHz range, such as those in Figure 1, were scanned. On spectrograms of this frequency scale, an ELF noise band is not easily distinguishable from ELF hiss.

If the scanning of the 0-8 kHz spectrogram of a given pass showed that an ELF noise band might be present, the tape for this pass was then run through the Spectran at four times the normal tape speed. This produced a spectrogram which was linear to about 1.2 kHz. Portions of spectrograms in this frequency range are shown in Figures 6 to 12.

From the scanning of these spectrograms the following qualitative characteristics were observed:

(1) Chorus is present at some time on nearly all passes for which ELF noise bands were observed. However, chorus and ELF noise bands are not necessarily present at the same time. It is possible that ELF noise bands and chorus can be simultaneously present, but that the ELF noise band cannot be detected. To show this, we must first recall that chorus observed in the high latitude regions has frequency components below 1.5 kHz. Also the response

of the wide band receiver falls off for lower frequencies. Thus, since the output from the wide band receiver is normalized, very strong chorus bursts could result in the loss of a detectable low frequency cutoff.

(2) The upper cutoff frequency components of the ELF noise bands are variable over a range of several hundred Hz. It is generally impractical to assign any upper frequency cutoff to the noise band, due to the presence of chorus. On 0-8 kHz spectrograms ELF hiss would often appear to have an upper frequency cutoff, but on 0-1.6 kHz spectrograms the upper frequency was found to be obscured by chorus.

An inspection of Missilyzer-sectionings, such as those shown in Figures 6-12, leads to the following conclusions:

(1) An abrupt change in intensity is often observed at the lower end of the spectrum. This noise band with an abrupt cutoff is defined as an ELF noise band. The frequency of the cutoff varies much less than the changes in the shape of the spectra. However, if Missilyzer-sectionings differing in time by a few minutes are compared, this cutoff is usually found to change monotonically.

(2) Frequency components below the cutoff usually have measurable amplitudes. However, the maximum amplitude of any frequency below the cutoff is smaller than the maximum amplitude of some frequencies less than 50 Hz above the cutoff. It is believed that much of this noise is not actual data received by the satellite,

but has been caused by noise in receiving and processing instruments. Figure 6 shows a Missilyzer-sectioning of an ELF noise band with a noise which is believed not to be of natural origin.

We may use the AGC reading and the 700 Hz spectral density measurement to get an idea of typical intensities. The AGC reading on approximately 5% of the ELF noise band events exceeded 7 milli-gamma, and for approximately 35% of the events, the reading was greater than 1.8mγ. ELF noise band events occurred both when the spectral density measurement at 700 Hz was below its background level (7×10^{-8} γ^2/Hz) and when it was at its maximum level (1.8×10^{-7} γ^2/Hz).

Since 380 Hz was set as a lower limit for which an F_c would be determined, a measure of the time duration of ELF noise bands was not possible. However, the passes which are studied in section 6 indicate ELF noise bands have a cutoff frequency for times of the order of five minutes. Again the presence of chorus bursts is a factor which hinders measurement.

In the investigation of ELF noise band, several other interesting phenomena were noticed. Of particular interest for their unusual appearance on frequency-time spectrograms are periodic emissions. Figure 13 shows parts of a spectrogram of a pass with this type of VLF emission present. Table I gives a list of passes on which periodic emissions were detected.

Most of the data taken used in this study were from passes in the northern hemisphere during the midyear of 1963 (revolutions 1700 to 2250). From Figure 5 we can see that the perigee of the satellite was in the southern hemisphere at this time. Since the multiple noise bands of Figure 4 occurred at low altitudes and high latitudes, the selection of sample data and the orbit of the satellite limited the possibility of finding multiple noise bands.

The proton whistler is a VLF noise which is a dispersed form of a lightning impulse. It usually has the same frequency range as ELF noise bands. However, in this investigation, there were no instances of simultaneous proton whistlers and ELF noise bands. It will be shown in Section 7, that a simultaneous presence would enable us to evaluate directly one hypothesis on the origin of ELF noise bands.

In order to propose and to evaluate any theoretical interpretation, we must select a characteristic of the ELF noise bands which can be measured and can test the hypotheses. By inspecting the various spectrograms and Missilyzer sectionings, F_c is seen to be probably the most useful parameter. In the next section, the region of the ionosphere and the time at which ELF noise bands occur most frequently are discussed.

5. STATISTICAL STUDY OF ELF NOISE BANDS

A large number of spectrograms were produced for studies of other VLF phenomena by Gurnett [1967], Pfeiffer [1966] and Oliven and Gurnett [1967]. These spectrograms, which covered a total of 627 passes, were taken as the sample for this investigation. The sample density is given in Table II. From this table it can be seen that the most intensely covered regions are the high altitude and mid-morning regions.

In order to learn what latitude and local time region most often contained ELF noise bands, the sample was divided into INV-MLT blocks. The number of revolutions for which an ELF noise band occurred was divided by the total number of revolutions through that block. The results are listed in Table III. In each block we have two numbers; the top one is the number of revolutions in the block for which ELF noise band events occurred; the bottom one is the percentage of revolutions with ELF noise band events. This table cannot be interpreted as giving the exact regions where ELF noise bands occur because of the following:

(1) The data in a given block is not time normalized; thus an ELF noise band event is more likely to occur in a given block on a pass which spends more time in this block than a pass which was

in the block for a smaller time interval. However, since ELF noise bands usually last throughout the entire time interval that a pass is in a block, the lack of time normalization may not be a serious factor.

(2) The restriction of F_c to frequencies above 380 Hz favors occurrences in the mid-latitude and low latitude regions. To show this, we must consider the range of altitudes in the INV-MLT blocks. Most of the high latitude data that were studied were received by Northern Hemisphere stations when perigee of the satellite was in the Southern Hemisphere. Later in this section, we show that F_c generally varies inversely with altitude. Thus by setting a lower limit on F_c we may have eliminated many measurements of the low frequency cutoff at high latitudes.

(3) The start and stop times given by ground stations for a satellite pass do not always correspond to the time when usable data was being received. Also this signal was lost near the end of many passes before the receiver was turned off. However, it can be reasonably assumed that this effect occurs evenly throughout the INV-MLT blocks. The net effect is that percentages shown in Table III are lower than the exact percentages.

(4) As was mentioned in the previous section, the presence of chorus may result in the loss of a detectable cutoff. Since chorus occurs most often in high latitude regions, we have another factor which tends to make the percentages shown in Table III lower

than the true values for high latitude regions.

Realizing these limitations, we may interpret Table III as showing that ELF noise bands most often occur in high latitude regions from mid-morning to early afternoon. In the MLT-INV region bounded by $6 < \text{MLT} \leq 11$ and $50° < \text{INV} \leq 70°$, the average percentage per block is 16.8%, while the overall percentage is 4%.

For ELF noise bands, the low frequency cutoffs may vary with the parameters of altitude, MLT and INV. In this part of the study, we will disregard variations of cutoffs with respect to MLT. Disregard of a parameter is necessary, since we want to consider variations which are determined by a significant number of events. In the next section, we will consider passes where the change in MLT during an ELF noise band event is not as great as the change in INV or altitude. Considering these passes to have typical orbits for passes with ELF noise bands, we feel that the variation of F_c with altitude within INV blocks gives the best approximation to its true variation.

This variation is shown in Figure 14. The INV blocks were divided into different sizes in order to try to keep a significant number of points in each of the blocks. A point in an INV block with some particular altitude and F_c tells us that at that altitude, noise with frequency components below F_c are not seen at the satellite. This result could possibly be interpreted as either that the source of noise does not generate frequencies below F_c at the

given altitude, or that the radiation with frequency components less than F_c cannot propagate at that given altitude. We will discuss this point again in section 7. For the 38°-50° INV block, we see that F_c is nearly independent of altitude, although there is a tendency for smaller F_c's to occur at higher altitudes. For the 50°-55° and 55°-60° INV blocks, the dependence of F_c on altitude is more marked. In the 60°-65° INV block the altitude dependence is less apparent, and an increasing amount of scatter has entered. In the 65°-70° INV block, the altitude dependence is very slight, and in the 70°-82° block it is negligible.

A physical quantity, which depends on altitude and latitude and has the dimensions of frequency, is the proton gyrofrequency Ω_p. We can normalize F_c by dividing by Ω_p and make a similar investigation of the variation of this new quantity (Λ) with altitude in INV blocks. The results of this investigation are shown in Figure 15.

In this figure we see that up to INV = 60°, we generally have $0.9 \leq \Lambda \leq 1.0$ for ELF noise bands at all altitudes. For the 60°-65° and 65°-70° INV blocks considerable scatter is introduced, although for most points $0.9 \leq \Lambda \leq 1.0$. However, the scatter decreases for the 70°-82° INV block.

In summary, ELF noise bands most often occur when $6 \leq$ MLT < 11 and $50° \leq$ INV $< 70°$. Also up to INV $\sim 60°$ F_c varies

nearly inversely with altitude. This means higher frequencies can be "cutoff" from the satellite at lower altitudes. At higher frequencies F_c becomes more independent with altitude, and there is increased scatter. When considering the variation of Λ, we find that usually $0.9 \leq \Lambda \leq 1.0$ for all altitudes, although the scatter is greatest for $60° \leq \text{INV} < 70°$.

6. INDIVIDUAL PASS STUDY

In contrast to the last section in which a large amount of the Injun III VLF data was considered, we limit ourselves in this section to three passes of the satellite. These passes are:

(1) Revolution 105, Station 00 (Iowa City)

(2) Revolution 775, Station 20 (Mojave, California)

(3) Revolution 1757, Station 02 (St. John's, Newfoundland, Canada) and Station 00.

These orbits in MLT-INV space are shown in Figure 16. The first two of these passes were selected because they contained clear examples of ELF noise bands and their orbits were quite different from each other. The last revolution was chosen since there were two different stations receiving VLF data at the same time.

(1) Revolution 105, Station 00

The 0-8 kHz and 0-1.6 kHz spectrograms, together with the variation of the orbital parameters, are shown in Figure 17. From the 0-8 kHz spectrogram, we can notice the distinct presence of chorus emissions from 15:20 to 15:24 (UT). ELF hiss can also be seen to be present throughout the entire interval shown in the figure, and discrete VLF emissions are apparent from 15:18 to 15:20 (UT). A careful inspection of the 0-1.6 kHz spectrogram

shows that ELF hiss bands have an F_c which goes above 380 Hz at UT $\simeq$ 15:19.

For UT greater than 15:22 and INV greater than 60°, an increasing amount of noise appears below the low frequency cutoff. At UT $\simeq$ 15:23 the low frequency cutoff is no longer detectable. In Figure 18, F_c and Ω_p are plotted against altitude, MLT and INV. From this plot we see that the difference in these frequencies decreases with increasing altitude, MLT and INV. This result might also be interpreted as follows: when the satellite goes to higher altitudes and latitudes it can receive frequency components which could not be received at lower altitudes and lower latitudes. Also we may note that Λ is decreasing with increasing altitude and decreasing latitude.

(2) Revolution 775, Station 20

An inspection of the 0-8 kHz spectrograms in Figure 19 shows that chorus is present from 16:20 to 16:24 (UT). A low frequency cutoff can also be identified on this spectrogram. The variation of F_c can be seen on the 0-1.6 kHz spectrogram. In Figure 20 we plot F_c and Ω_p versus our parameters of altitude, MLT and INV. We note that for increasing altitudes and decreasing latitudes, F_c and Λ decrease. Also the cutoff becomes clearer for INV < 60°. Hence, at higher altitudes and lower latitudes, the satellite is receiving

noise with frequency components too low to be received at lower altitudes and higher latitudes.

(3) Revolution 1757, Stations 00 and 02

The reception for this pass by Station 02 was rather poor (as shown by the spectrograms in Figure 21). Thus, we have included, for this pass, spectrograms (Figure 22) of the VLF data received by a different tracking station (Station 00). This has been done to illustrate a very useful test for the validity of the data - the comparison of data received simultaneously by different tracking stations. The background noise in the spectrogram for Station 02 nearly obscures the chorus emissions, which are clearly seen in the 0-8 kHz spectrogram of the data from Station 00. However, towards the end of the 0-1.6 kHz spectrograms of data received by Station 02, we find a possible continuation of the ELF noise band that is easily seen on the beginning of the 0-1.6 kHz spectrogram of Station 00. This ELF noise band is less apparent at the beginning of the Station 02 data. A very careful inspection of the 0-1.6 kHz spectrogram indicates that it is probable that the ELF noise band was present for the 11 minutes of UT for 13:52 to 14:03. Over this interval, MLT varied from 9 hrs to 15 hrs, INV from 55° to 73.5° and the altitude from 600 km to 1300 km. This, clearly, is a very wide range.

In Figure 23, we plot the variation of Ω_p and F_c with respect to altitude, MLT and INV. For the first part of the

pass, we note that F_c increases with increasing altitude and latitude until INV > 57°, when the ELF noise band becomes difficult to identify. After the satellite reaches its maximum latitude at UT $\simeq$ 14:00 , F_c decreases slowly with increasing altitude and slightly decreasing latitude. For the beginning portion of the pass, we see that Λ decreases with increasing UT, but at the end of the pass Λ may increase slightly.

Making comparisons between these three passes we may conclude:

(1) For increasing altitudes, F_c and Λ usually decrease. The exception to this pattern was a case where Λ increased slightly at high latitudes.

(2) For all passes there was difficulty in measuring the low frequency cutoff when INV was greater than 60°. This result of the individual pass investigation may have an analogous result in the statistical study, namely the increased scatter in regions for which INV > 60°.

7. POSSIBLE INTERPRETATIONS OF ELF NOISE BANDS

Noise bands in the audio-frequency range have been the object of ground observations by Ungstrup [1959], Egeland [1959], Pope [1960], Gustafsson et al. [1962], Ungstrup and Jackerott [1963] and Egeland et al. [1965]. The ground stations have been located in the auroral zone and the maximum time of occurrence for noise in the 1 kHz range is usually in the late morning. These investigators have most often found the peak of the noise band to be around 750 Hz, and thus their observations may support the hypothesis of Aarons [1960], that the source of this noise is cyclotron radiation from protons at altitudes from 200 km to 400 km.

The results of the statistical study have shown that the cutoffs of ELF noise bands are most often below and within 10% of the proton gyrofrequency and that ELF noise bands occur most often at high latitudes in the late morning. Hence proton cyclotron radiation can be reasonably proposed as a source of ELF noise bands. However the points in Figure 14 show that for given altitudes, no frequency components of the noise source which are less than F_c for that altitude have reached the satellite. There is no direct connection between the peak frequency and F_c. Hence rather than

reviewing the theories of generation of VLF and ELF radio noise, we will determine if the cutoff may be due to a propagation effect of radiation from an unknown source.

It is possible to determine quantitatively the properties of electromagnetic wave propagation in the ionosphere by treating the ionosphere as a cold plasma. For definiteness we assume a diffusive equilibrium model ionosphere with three types of ions (H^+, He^+ and O^+). The variation of the electron number density and ion number densities with altitude for this model ionosphere we will use for this discussion is shown in Figure 24. It should be noted that the ion concentrations for this model agree best with experimental measurements made in the mid-latitude region at night.

In the appendix we derive the result, given by Stix [1962], that there can be no propagation for a left hand polarized wave when the index of refraction for that frequency passes below its $L = 0$ surface. Gurnett [1965] observed the possible effects of this cutoff and hypothesized that the cutoffs of the noise bands shown in Figure 4 are due to reflection of waves emitted by a source at high altitudes. Applying this hypothesis for waves emitted from a "white noise" source at high altitudes, we can expect to observe noise bands with a sharp low frequency cutoff which varies in altitude.

In order to determine the variation of the frequency for which $L = 0$ ($F(L = 0)$), we use the model ionosphere given in

Figure 24. We then calculate the variation of $F(L = 0)$ with altitude. Figure 25 shows the result of this calculation for latitudes of 30° and 60°. We can also see by an inspection of equation A-20 that $F(L = 0)/\Omega_p$ must be less than unity.

We can now compare the predictions of the "L = 0" hypothesis with the experimental results given in Figures 14 and 15. Comparing Figures 25 and 14, we see that for the lowest INV block, we have agreement between the "L = 0" hypothesis and the experimental data. However for higher INV, we find that for a given altitude F_c is generally much less than $F(L = 0)$. From Figure 15 we see that experimental points have been measured for which we have $\Lambda > 1.0$. These cutoffs cannot be due to L = 0. These cutoffs may be due to a source effect.

We should now investigate the dependence of the predicted behavior on the choice of a model ionosphere. If the fractional concentration of hydrogen ions (α) was much lower than has been assumed, then we can see from the inequality relation A-32 that Λ would be closer to 1. A sharp decline in α for the high latitude region has been reported by Barrington et al. [1965].

It has been shown by Shawhan and Gurnett [1966] that spectrograms of proton whistlers can be used to measure α to within 3%. Thus if an ELF noise band and a proton whistler occurred simultaneously, we could compare α values calculated from both events and compare these values. However since proton whistlers occur mostly near midnight below 45° and ELF noise bands occur

generally in the morning at high latitudes simultaneous occurrences would not be frequent, and have not yet been found.

It is possible that the cutoff of ELF noise bands could be due to a combination of source and propagation effects. This would mean that only above the low frequency cutoff of the source could we observe a cutoff due to propagation effect. It has also been suggested by Shawhan [1967] that "trapped waves" can account for the noise in the ELF region. The cutoff of these waves can be above the proton gyrofrequency.

8. CONCLUSIONS

For this study we have called those ELF hiss bands with a sharp low frequency cutoff ELF noise bands. We first investigated the spectral characteristics of these noise bands. For nearly all passes on which ELF noise bands occurred, chorus events took place. Intense chorus bursts may have resulted in the loss of detectability of the low frequency cutoff at times. Multiple noise bands were found only when the satellite was at a low altitude in a high latitude region.

The ELF noise bands occurred over a wide range of AGC readings and 700 Hz spectral density measurements. However, in MLT-INV space the average percent occurrences in region defined by $6 \leq \text{MLT} < 11$ and $50° \leq \text{INV} < 70°$ were four times as frequent as the average outside this region.

An investigation of the variation of F_c in INV blocks showed that there was a marked dependence on altitude only up to INV = 60°. The plots of cutoff frequency versus altitude may be interpreted as showing at what altitudes frequencies below F_c were not received by the satellite.

An investigation of the variation of Λ in the INV blocks showed that the greatest departure from the limits $0.9 \leq \Lambda \leq 1.0$ occurred in the 60°-70° blocks. A general systematic decrease of

F_c with increasing altitude was found in a study of three individual passes.

The cutoff can be interpreted as being either a source effect or a propagation effect. A cutoff effect due to the index of refraction for left hand polarized waves was proposed a propagation effect. There was agreement for the lowest INV block, and at higher latitudes the cutoffs were generally lower than those calculated using a midlatitude model ionosphere. Points for which $\Lambda > 1.0$ were interpreted as indicating the cutoffs may be due to more than one cause or to source effects.

APPENDIX

In order to derive the dispersion relation for a plasma we first make a few simplifying assumptions.

(1) Zero order quantities such as the density and composition of the plasma are constant in space and time.

(2) First order quantities vary as $\exp[i(\vec{k}\cdot\vec{r} - \omega t)]$

(3) The plasma is collisionless.

Assumption (3) allows us to use Vlasov's equation for the k^{th} species of the plasma:

$$\frac{\partial f_k}{\partial t} + \vec{U}\cdot\nabla_{\vec{r}} f_k + \frac{F}{m_k}\cdot\nabla_{\vec{u}}(f_k) = 0 \qquad (1)$$

where $F = q_k(\vec{E} + \vec{v}_k \times \vec{B}) = \epsilon_k e\left(\vec{E} + \frac{\vec{v}_k \times \vec{B}}{c}\right)$.

Taking the zeroth moment of the Vlasov equation we get the equation of continuity:

$$\frac{\partial n_k}{\partial t} + \nabla_{\vec{r}} \cdot (n_k \vec{v}_k) = 0 \qquad (2)$$

Taking the first moments of the Vlasov equation we get Euler's equation with the Lorentz force term

$$m_k n_k\left[\frac{\partial \vec{v}_k}{\partial t} + (\vec{v}_k\cdot\nabla_{\vec{r}})\vec{v}_k\right] = n_k \epsilon_k e\,(\vec{E} + \vec{v}_k \times \vec{B}) - \nabla\cdot(\vec{P}_k) \qquad (3)$$

where $\vec{\vec{P}}_k = m_k \int f_k \, (\vec{u} - \vec{v}_k)\,(\vec{u} - \vec{v}_k)\, d\vec{u}$

For a "cold plasma", we set $\nabla \cdot (\vec{\vec{P}}_k) = 0$.

Equation (3) then becomes:

$$m_k \left[\frac{\partial \vec{v}_k}{\partial t} + (\vec{v}_k \cdot \nabla_{\vec{r}})\, \vec{v}_k \right] = \epsilon_k \, e \left(\vec{E} + \frac{\vec{v}_k \times \vec{B}}{c} \right) . \tag{4}$$

Making use of assumptions (1) and (2) and assuming no net zero order streaming (i.e., $\vec{v}_k = \vec{v}_k^{(1)}$), and small amplitude waves ($\vec{E} = \vec{E}^{(1)}$), we can solve for $\vec{v}^{(1)}$ in terms of the electric field. The result when written in matrix form is:

$$\begin{pmatrix} v_{k,1}^{(1)} \\ v_{k,2}^{(1)} \\ v_{k,3}^{(1)} \end{pmatrix} = \frac{\epsilon_k \, e}{m_k} \begin{pmatrix} \frac{-i\omega}{\Omega_k^2 - \omega^2} & \frac{-\epsilon_k \, \Omega_k}{\Omega_k^2 - \omega^2} & 0 \\ \frac{\epsilon_k \, \Omega_k}{\Omega_k^2 - \omega^2} & \frac{-\, i\, \omega}{\Omega_k^2 - \omega^2} & 0 \\ 0 & 0 & i/\omega \end{pmatrix} \begin{pmatrix} E_1^{(1)} \\ E_2^{(1)} \\ E_3^{(1)} \end{pmatrix} \tag{5}$$

where $\Omega_k = \dfrac{eB_o}{m_k c}$.

The net current is given by:

$$\vec{J}^{(1)} = \sum_k \epsilon_k \, e \, n_k \, \vec{v}_k^{(1)} \quad . \tag{6}$$

Generalizing Ohm's law, we define a complex conductivity tensor by:

$$\vec{J}^{(1)} = \vec{\vec{\sigma}} \cdot \vec{E}^{(1)} \tag{7}$$

Putting equation (5) into equation (6), we find that the conductivity tensor is given by

$$\overleftrightarrow{\sigma} = \sum_k \frac{n_k e^2}{m_k} \begin{pmatrix} \frac{-i\omega}{\Omega_k^2-\omega^2} & \frac{-\epsilon_k \Omega_k}{\Omega_k^2-\omega^2} & 0 \\ \frac{\epsilon_k \Omega_k}{\Omega_k^2-\omega^2} & \frac{-i\omega}{\Omega_k^2-\omega^2} & 0 \\ 0 & 0 & \frac{i}{\omega} \end{pmatrix} . \qquad (8)$$

The relationship between the dielectric tensor and the conductivity tensor is given by:

$$\overleftrightarrow{K} = \overleftrightarrow{1} - 4\pi\overleftrightarrow{\sigma}/i\omega \qquad (9)$$

Therefore, using the notation of Stix [1962], we can write the dielectric tensor as

$$\overleftrightarrow{K} = \begin{bmatrix} S & -iD & 0 \\ iD & S & 0 \\ 0 & 0 & P \end{bmatrix} \qquad (10)$$

where

$$S = 1 - \sum_k \frac{\pi_k^2}{\omega^2-\Omega_k^2} \qquad (11)$$

$$D = \sum_k \frac{\epsilon_k \Omega_k}{\omega} \frac{\pi_k^2}{\omega^2-\Omega_k^2} \qquad (12)$$

and $$\pi_k^2 = \frac{4\pi n_k e^2}{m_k}$$

Also we may define

$$R = S + D = 1 - \sum_k \frac{\pi_k^2}{\omega(\omega+\epsilon_k\Omega_k)} \tag{13}$$

$$L = S - D = 1 - \sum_k \frac{\pi_k^2}{\omega(\omega-\epsilon_k\Omega_k)} \tag{14}$$

With assumption (2) the first two Maxwell equations can be written as:

$$i\,\vec{k} \times \vec{E} = i\omega\,\vec{B}/c \tag{15}$$

$$i\,\vec{k} \times \vec{B} = \frac{i\omega\,\vec{D}}{c} = \frac{-i\omega}{c}\,\vec{\vec{K}}\cdot\vec{E} \quad . \tag{16}$$

Taking the cross product of (15) with $\vec{k}$ and substituting the results in (16) we have

$$\vec{k} \times (\vec{k} \times \vec{E}) + \frac{\omega^2}{c^2}\,\vec{\vec{K}}\cdot\vec{E} = 0 \quad . \tag{17}$$

Letting $\vec{n} = \frac{\vec{k}C}{\omega}$, equation (17) becomes

$$\vec{n} \times (\vec{n} \times \vec{E}) + \vec{\vec{K}}\cdot\vec{E} = 0 \tag{18}$$

Letting $\vec{B}_o = \hat{e}_3 B_o$ and assuming $\hat{n}$ to be in the 1-3 plane, equation (18) in matrix form becomes:

$$\begin{pmatrix} S-n^2\cos^2\theta & -i\,D & n^2\cos\theta\sin\theta \\ i\,D & S-n^2 & 0 \\ n^2\cos\theta\sin\theta & 0 & P-n^2\sin^2\theta \end{pmatrix} \begin{pmatrix} E_1 \\ E_2 \\ E_3 \end{pmatrix} = 0 \qquad (20)$$

Where θ is the angle between $\vec{B}$ and $\vec{n}$.

The condition for equation (20) to have a non-trivial solution is that the determinant of the 3 x 3 matrix be zero. For this to be true, we must have:

$$n^4(S\sin^2\theta + P\cos^2\theta) + n^2(D^2\sin^2\theta - SP\cos^2\theta - S^2\sin^2\theta - SP) + P(S^2 - D^2) = 0 \; . \qquad (21)$$

This is the dispersion relation.

From equations (13) and (14) we have that

$$S^2 - D^2 = RL \; . \qquad (22)$$

Thus the dispersion relation can be written as:

$$n^4(S\sin^2\theta + P\cos^2\theta) - n^2[RL\sin^2\theta + SP(1 + \cos^2\theta)] + RPL = 0 \; . \qquad (23)$$

For $\theta = 0$ equation (23) becomes

$$n^4 P - n^2(R + L)P + PRL = 0 \; .$$

Thus the conditions which can hold at $\theta = 0$ are:

$$P = 0$$

$$n^2 = R$$

$$n^2 = L \; .$$

In order to interpret R and L, consider the second line of (20). This can be written as:

$$i\,D\,E_1^{(1)} + (S - n^2)\,E_2^{(1)} = 0$$

$$\text{or} \qquad \frac{iE_1^{(1)}}{E_2} = \frac{n^2 S}{D} = \frac{\frac{1}{2}(R + L) - n^2}{\frac{1}{2}(R - L)} \quad . \tag{24}$$

Thus for $n^2 = R$ equation (24) becomes

$$\frac{i\,E_1^{(1)}}{E_2} = 1$$

and for $n^2 = L$ it becomes

$$\frac{i\,E_1^{(1)}}{E_2} = -1 \quad .$$

The first case is known as right-hand polarization while the second is known as left-hand polarization. Hence L is the index of refraction for a left-hand polarized wave, and R is the index of refraction for a right-hand polarized wave.

The solution to the equation (21) can be written as:

$$n^2 = \frac{RL \sin^2\theta + PS(1 + \cos^2\theta) \pm \sqrt{(RL - PS)^2 \sin^4\theta + 4P^2(S^2 - RL)\cos^2\theta}}{2(S \sin^2\theta + P \cos^2\theta)} . \tag{25}$$

If we choose the - sign in (25) and set $L = 0$, then we get $n^2 = 0$. Also when $L = 0$, $n^2 = 0$; hence the choice of a - sign in (25) means we are considering left-hand circularly polarized waves.

Let us consider left-hand polarized waves with RL = ϵ and $\epsilon \ll PS$. Equation (25) then becomes

$$n^2 = \frac{\epsilon \sin^2\theta + PS\,(1 + \cos^2\theta) - \sqrt{(\epsilon - PS)^2 \sin^4\theta + 4P^2(S^2 - \epsilon)\cos^2\theta}}{2(S \sin^2\theta + P \cos^2\theta)} . \tag{26}$$

Expanding the terms in the square root, we get

$$n^2 \simeq \frac{2\epsilon PS \sin^2\theta - \epsilon^2 \sin^4\theta + 2P^2\epsilon \cos^2\theta}{2PS\,(1 + \cos^2\theta)\,(S \sin^2\theta + P \cos^2\theta)}$$

$$\simeq \frac{2\epsilon P\,(S \sin^2\theta + P \cos^2\theta)}{2\,PS\,(1 + \cos^2\theta)\,(S \sin^2\theta + P \cos^2\theta)}$$

$$= \frac{\epsilon}{S(1 + \cos^2\theta)} . \tag{27}$$

If we have $|R| > |L|$ and $L > 0$ then $n^2 > 0$ for all θ. But if $L < 0$, then $n^2 < 0$ for all θ.

This means that for left-hand polarized waves near the region where $L = 0$, we have propagation if $L = 0$ and evanescence if $L < 0$. Hence the surface $L = 0$ acts as a cutoff for left-hand polarized waves at all angles. This result was given by Stix [1962].

We now wish to determine at what ion concentrations we have the condition $L = 0$. We first introduce the following notation:

$\Lambda_1 = \omega/\Omega_p$

n_e = electron number density

$n(H^+)$ = hydrogen ion number density

$n(He^+)$ = helium ion number density

$n(O^+)$ = oxygen ion number density

$$\alpha = \frac{n(H^+)}{n_e}$$

$$\beta = \frac{n(He^+)}{n_e}$$

$$\delta = \frac{n(O^+)}{n_e} \quad .$$

In a plasma containing only electrons and H^+, He^+ and O^+ ions, (14) can be written as:

$$L = 1 + \left(\frac{\pi_e}{\Omega_e}\right)^2 + \frac{\pi_e^2}{\Omega_p \Omega_e}\left[\frac{1}{\Lambda_1} - \frac{\alpha}{\Lambda_1(1-\Lambda_1)} - \frac{\beta}{\Lambda_1(1-4\Lambda_1)} - \frac{\delta}{\Lambda_1(1-16\Lambda_1)}\right] . \tag{28}$$

For charge neutrality we must have $\alpha + \beta + \delta = 1$. With this condition (28) can be written as:

$$L = 1 + \left(\frac{\pi_e}{\Omega_e}\right)^2 + \frac{\pi_e^2}{\Omega_p \Omega_e}\left[\frac{1}{\Lambda_1}\left(1 - \frac{1}{1-16\Lambda_1}\right) - \frac{\alpha}{\Lambda_1}\left(\frac{1}{1-\Lambda_1} - \frac{1}{1-16\Lambda_1}\right)\right.$$

$$\left. + \frac{\beta}{\Lambda_1}\left(\frac{1}{1-4\Lambda_1} - \frac{1}{1-16\Lambda_1}\right)\right] . \tag{29}$$

Following the method of Gurnett [1965] we note that

$$\Omega_e \gg \Omega_p$$

and when the electron number density is not very small

$$\left(\frac{\pi_e}{\Omega_e}\right)^2 \gg 1 \quad .$$

Using these approximations we may write (29) as:

$$L \simeq \frac{\pi_e^2}{\Omega_p \Omega_e \Lambda_1 (1-16\Lambda_1)} \left[-16\,\Lambda_1 + \frac{\alpha\, 15\Lambda_1}{1-\Lambda_1} + \frac{\beta\, 12\Lambda_1}{1-4\Lambda_1} \right] . \qquad (30)$$

Thus an approximate condition for L = 0 is:

$$\frac{15\alpha}{1-\Lambda_1} + \frac{12\beta}{1-4\Lambda_1} = 16 . \qquad (31)$$

This equation gives:

$$\frac{16}{15}(1-\Lambda_1) < \alpha < \frac{4}{3}(1-\Lambda_1) \qquad (32)$$

as the limits for α .

TABLE I

ELF PERIODIC EMISSIONS

Rev	Universal Time		Invariant Latitude		Local Time		Altitude	
	Start	Stop	Start	Stop	Start	Stop	Start	Stop
1773	2043	2048	56.8	70.0	9.9	12.9	875	1330
1800	0103	0106	55.7	55.3	18.2	18.7	2440	2555
1973	2117	2120.5	73.7	71.2	13.5	14.3	2133	2290
1974	2310	2331	69.3	46.3	9.9	16.1	2017	2687
1978	0635	0639	50.4	60.1	6.2	8.6	997	1538
2035	2030	2033	66.3	61.1	14.1	14.5	2530	2610
2152	0451	0456	67.6	67.9	6.2	8.3	1877	2160
2308	1633	1636	68.9	64.5	9.9	10.2	2665	2670
3750	1821	1825	76.2	75.9	10.7	12.5	850	1118

TABLE II

SAMPLE DENSITY

INV / MLT	10°-20°	20°-30°	30°-40°	40°-50°	50°-60°	60°-70°	70°-80°	80°-90°
0-1	4	6	25	26	19	25	31	9
1-2	4	8	16	19	25	33	26	5
2-3	2	12	21	26	18	28	29	6
3-4		4	22	23	24	27	40	5
4-5	1	8	18	25	25	27	47	4
5-6	2	5	34	30	33	40	45	2
6-7		4	35	32	44	52	58	2
7-8	1	1	30	31	39	67	65	2
8-9		2	16	34	44	78	83	4
9-10		2	19	17	35	85	90	6
10-11		2	10	9	26	70	95	7
11-12			8	18	28	48	81	17
12-13	2	5	19	21	12	35	69	17
13-14	1	12	21	19	20	28	62	14
14-15	3	12	20	24	27	28	67	10
15-16	1	11	18	20	15	30	52	7
16-17		16	14	21	19	29	45	2
17-18	3	16	17	18	22	38	40	7
18-19	2	10	14	19	29	34	38	6
19-20	3	12	22	18	17	18	35	2
20-21	3	11	19	23	27	36	40	4
21-22	5	18	28	27	19	42	30	5
22-23	5	11	29	24	20	34	37	9
23-24	2	9	23	24	22	20	33	11

TABLE III

DENSITY OF OCCURRENCE

INV / MLT	30°-40°	40°-50°	50°-60°	60°-70°	70°-80°	80°-90°
3-4				3 11%	3 11%	
4-5				2 7.4%	4 8.5%	
5-6			1 3%	1 2.5%	1 2.2%	2 100%
6-7	1 3%	2 6%	4 9%	4 7.6%	1 1.7%	
7-8		1 3.2%	8 20.4%	9 13.4%	2 3%	
8-9		2 5.8%	20 45.4%	10 12.8%	3 3.6%	
9-10		1 5.8%	7 20%	17 20%	2 2.2%	
10-11			2 7.6%	10 14.2%	6 7.4%	2 28%
11-12			1 3.5%	4 8.3%		1 8.3%
12-13			1 8.3%		4 5%	1 5.8%
13-14			2 10%	1 3.5%	4 5.1%	1 5.8%
14-15			1 3.7%	2 7.1%	1 3.2%	2 20%
15-16			2 13.3%	1 3.3%	4 7%	
16-17		1 4.7%	1 5.3%	1 3.4%	1 2.2%	
17-18		1 5.5%			1 2.5%	
18-19		1 5.2%			1 2.9%	
19-20		2 11%				

REFERENCES

Aarons, J., G. Gustafsson and A. Egeland, Correlation of audio-frequency electromagnetic radiation with auroral zone micropulsations, Nature, 185, 148, 1960.

Allcock, G. McK., A study of the audio-frequency radio phenomena known as dawn chorus, Australian J. Phys., 10, 286-298, 1957.

Barrington, R. E., J. S. Belrose and G. L. Nelms, Ion composition and temperatures at 1000 km as deduced from simultaneous observations of a VLF plasma resonance and topside sounding data from the Alouette I satellite, J. Geophys. Res., 70, 1647-1664, 1965.

Brice, N., Discrete VLF emissions from the upper atmosphere, Standford Electronics Laboratory Technical Report 3412-6, 1964.

Chamberlain, J. W., Physics of the Aurora and Airglow, New York, Academic Press, 1961.

Egeland, A., G. Gustafsson, S. Olsen, W. Barron and A. Katz, An investigation of the natural electromagnetic radiation between 10 c/s and 10 kc/s, Arkiv för Geopysik, 4, 537-562, 1964.

Ellis, G. R. A., Low frequency electromagnetic radiation associated with magnetic disturbances, J. Planetary and Space Science, 1, 253, 1959.

Gallet, R. M., The-very-low-frequency emissions generated in the earth's exosphere, Proc. IRE, 47, 211-231, 1959.

Gurnett, D. A., Very low frequency electromagnetic emissions observed with the O.N.R./S.U.I. satellite Injun III, SUI Research Report 63-27, 1963.

Gurnett, D. A. and B. J. O'Brien, High latitude geophysical studies with satellite Injun 3. 5. Very-low-frequency electromagnetic radiation, J. Geophys. Res., 69, 65-89, 1964.

Gurnett, D. A., Ion cyclotron whistlers, SUI Research Report 65-2, 1965.

Gurnett, D. A., A satellite study of VLF hiss, J. Geophys. Res., 71, 5599-5615, 1966.

Gustafsson, G. A., A. Egeland and J. Aarons, Audio-frequency electromagnetic radiation in the auroral zone, J. Geophys. Res., 65, 2749-2578, 1960.

Helliwell, R. A., J. P. Katsufrakis, K. E. Marks, D. Reed and M. L. Trimpi, An atlas of selected VLF spectra from Byrd Station, Antartica, Standford Electronics Laboratory Technical Report 62-046, 1962.

Helliwell, R. A., Whistlers and Related Ionospheric Phenomena, Standford University Press, Standford, California, 1965.

McIllwain, C. E., Coordinates for mapping the distribution of magnetically trapped particles, J. Geophys. Res., 66, 3681-3691, 1961.

O'Brien, B. J., C. D. Laughlin and D. A. Gurnett, The Injun III satellite, SUI Research Report 62-24, 1962.

Oliven, M. N. and D. A. Gurnett, Microburst phenomena 3. VLF chorus-microburst correlation, to be published, J. Geophys. Res., 1967.

Pfeiffer, G. W., Non-Eckersley's law whistlers observed with satellite Injun III, Master's Thesis, Department of Physics and Astronomy, University of Iowa, Iowa City, Iowa, August, 1966.

Pope, J. H., Diurnal variation in the occurrence of "Dawn Chorus", Nature, 180, 433, 1957.

Pope, J. H., Effects of latitude on the diurnal maximum of "Dawn Chorus", Nature, 185, 87-88, 1960.

Shawhan, S. D. and D. A. Gurnett, Fractional concentration of hydrogen ions in the ionosphere from VLF proton whistler meacurements, J. Geophys. Res., 71, 47-59, 1966.

Shawhan, S. D., VLF ray tracing in a model ionosphere, SUI Research Report 66-33, 1966.

Stix, T. H., The theory of plasma waves, McGraw Hill Book Co., Inc., New York, 1962.

Storey, L. R. D., An investigation of whistling atmospherics, Phil. Trans. Roy. Soc., A, 246, 113-141, 1953.

Ungstrup, E., Observations of whistlers and very low frequency phenomena at Godhaven, Greenland, Nature, 184, 806, 1959.

Ungstrup, E. and I. M. Jackerott, Observations of chorus below 1500 cycles per second at Godhaven, Greenland from July 1957 to December 1961, J. Geophys. Res., 68, 2141-2146, 1963.

FIGURE CAPTIONS

Figure 1. Two spectrograms of ELF hiss found in the Injun III VLF experimental data. For both cases the hiss events last more than 1 minute. During this time the spectral characteristics do not change greatly.

Figure 2. Two spectrograms of VLF chorus found in the Injun III VLF experimental data. The chorus present on revolution 1845 has lower frequency components than the chorus on revolution 3786. Both cases of chorus last longer than a minute.

Figure 3. Frequency response of the wide-band VLF system. The response gradually falls off for frequencies less than one kHz.

Figure 4. Two spectrograms of radio noise emissions at frequencies below 1.5 kHz. Two low-frequency cutoffs can be noticed for each of the emissions.

Figure 5. The variation of Injun III's perigee with revolution. The majority of data used in this investigation was from revolution 1750-2250.

Figures 6-12. Missilyzer-sectioning and 0-8 kHz and 0-1.6 kHz spectrograms for ELF noise band events which occur over a wide range of magnetic field signal strength and 700 Hz spectral density measurements.

Figure 13. Portions of spectrograms for a periodic emission event. ELF hiss is present during the entire event.

Figure 14. Low frequency cutoff plotted against altitude for six INV blocks. For a given altitude and cutoff frequency a data point indicates that noise with frequency components less than the cutoff frequency was not received by the satellite.

Figure 15. The ratio of the cutoff frequencies to the proton gyrofrequency plotted versus altitude for six INV blocks.

Figure 16. Orbits in INV-MLT space for the passes selected for the individual pass study.

Figure 17. The 0-8 kHz and 0-1.6 kHz spectrograms for revolution 105, Station 00. The orbital parameters of the satellite for this time are given.

Figure 18. The cutoff frequency and proton gyrofrequency plotted against the orbital parameters of the satellite. Only the altitude scale is linear.

Figure 19. The 0-8 kHz and 0-1.6 kHz spectrograms for revolution 775, Station 20. The orbital parameters of the satellite for this time are given.

Figure 20. The cutoff frequency and proton gyrofrequency plotted against the orbital parameters of the satellite. Only the altitude scale is linear.

Figure 21. The 0-8 kHz and 0-1.6 kHz spectrograms for revolution 1757, Station 02. The orbital parameters for the satellite for this time are given.

Figure 22. The 0-8 kHz and 0-1.6 kHz spectrograms for revolution 1757, Station 00. The orbital parameters for the satellite for this time are given.

Figure 23. The cutoff frequency and proton gyrofrequency plotted against the orbital parameters of the satellite.

Figure 24. Mid-latitude diffusive equilibrium model ionosphere.

Figure 25. The frequency at which L = 0 plotted against altitude for latitudes of 30 and 60 degrees. The model ionosphere of Figure 24 has been used in the calculations.

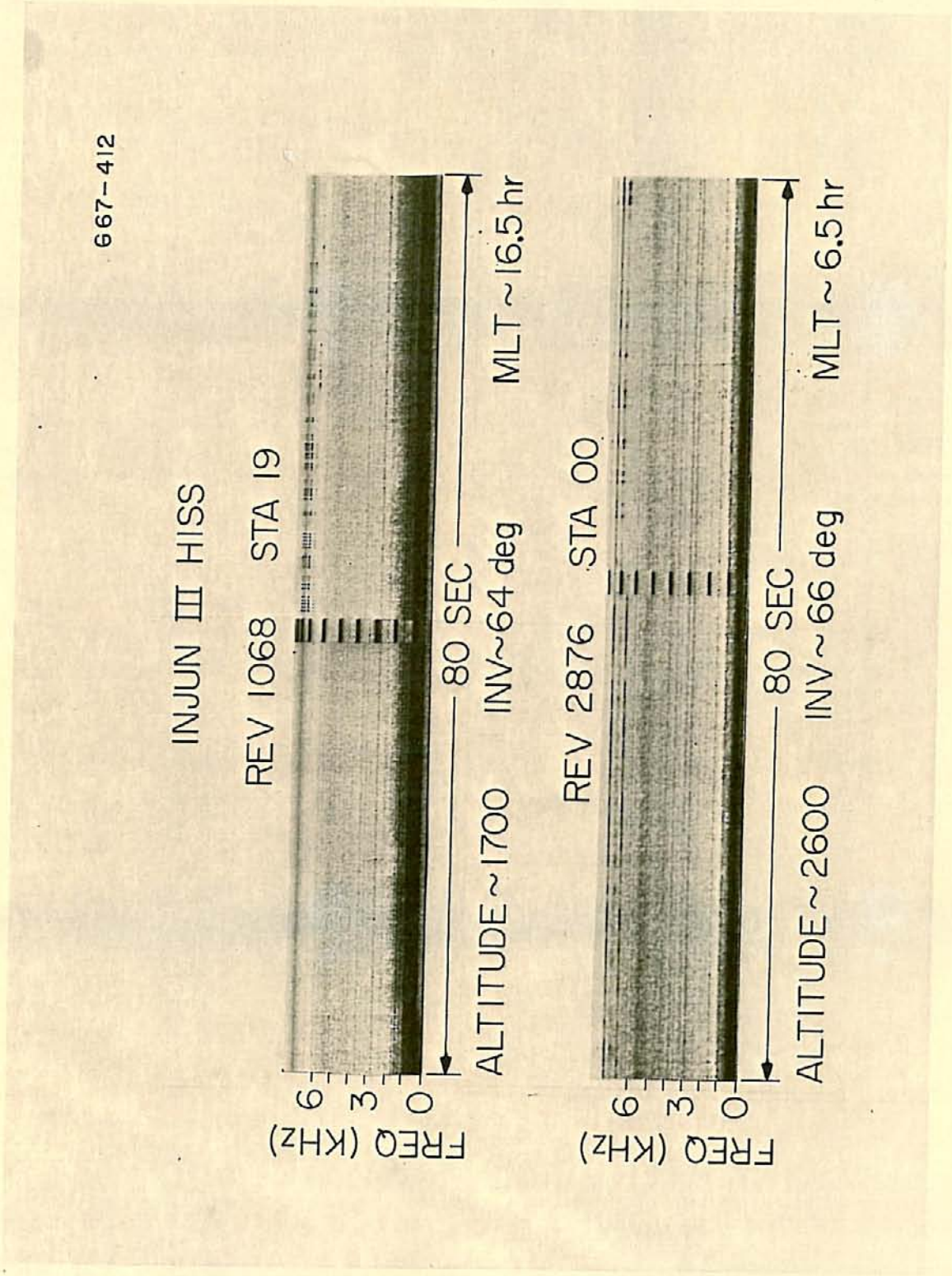
667-412
INJUN III HISS
REV 1068 STA 19
FREQ (KHz)
9
3
0
80 SEC
ALTITUDE ~ 1700
INV ~ 64 deg
MLT ~ 16.5 hr
REV 2876 STA 00
FREQ (KHz)
9
3
0
80 SEC
ALTITUDE ~ 2600
INV ~ 66 deg
MLT ~ 6.5 hr

FIGURE 1

G67-413

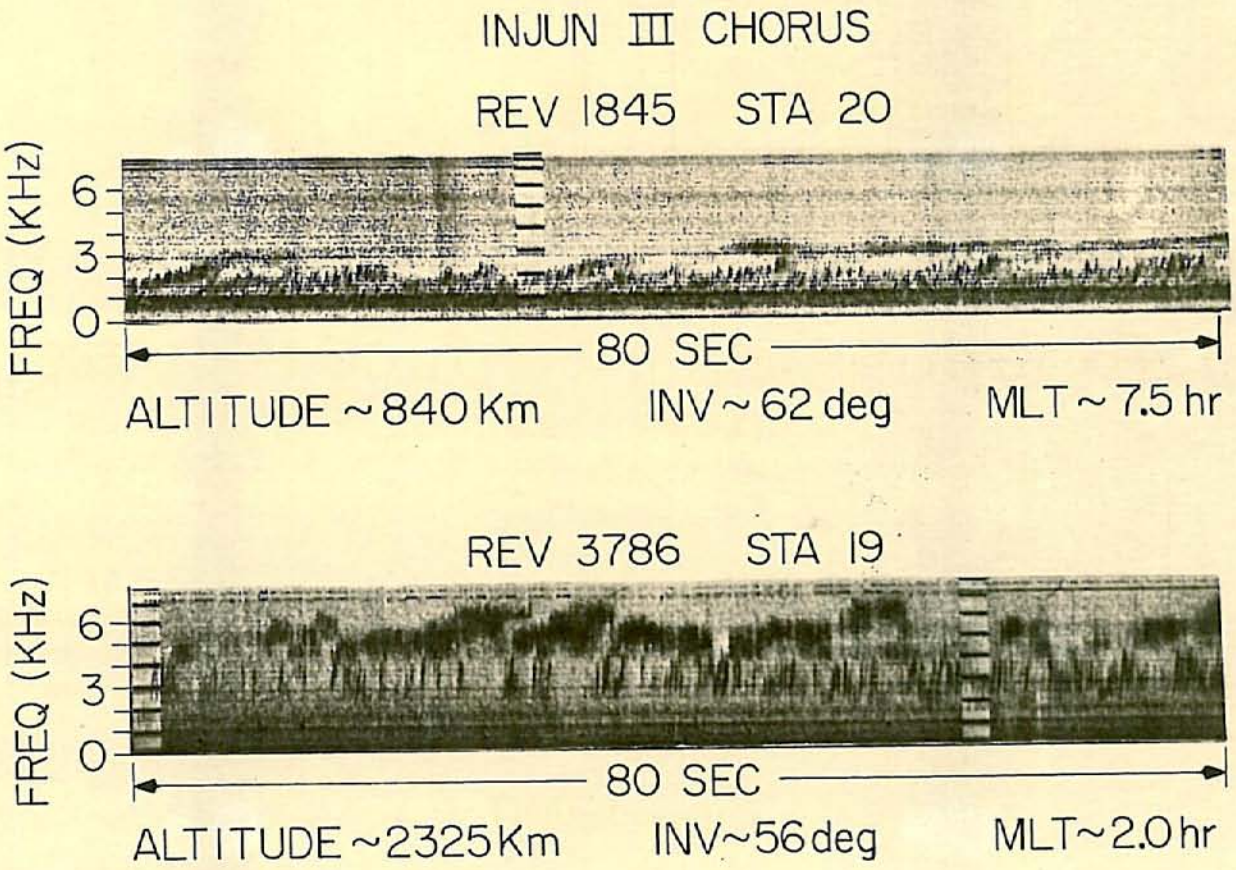

FIGURE 2

JAN. 14, 1963 10:46:10 UT, 05:20LT, ALTITUDE = 640 Km
L = 7.2 Ω_1 = 675 c/s.

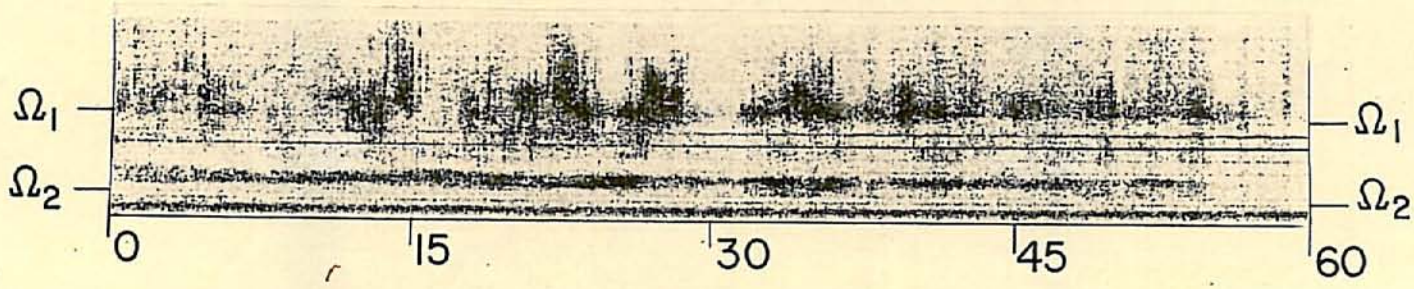

JAN. 17, 1963, 10:24:00 UT, 05:11LT ALTITUDE = 527 Km
L = 9.9 Ω_1 = 725 c/s.

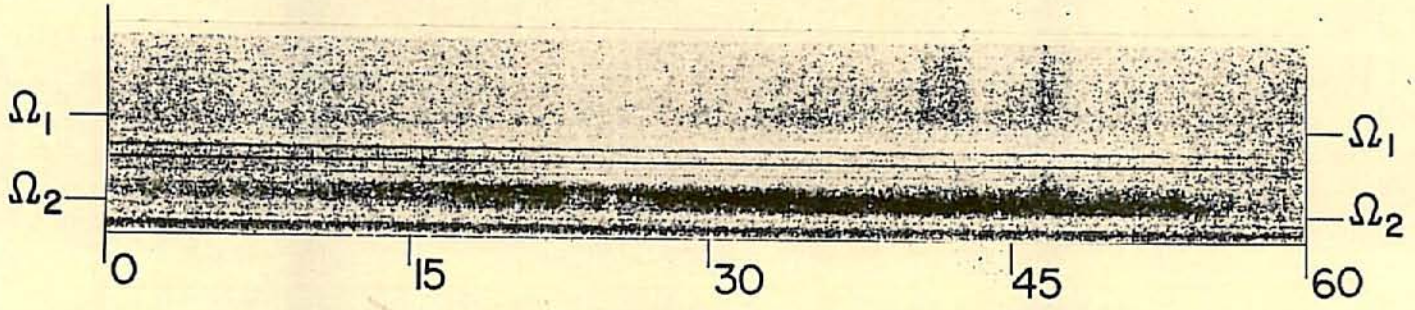

FIGURE 3

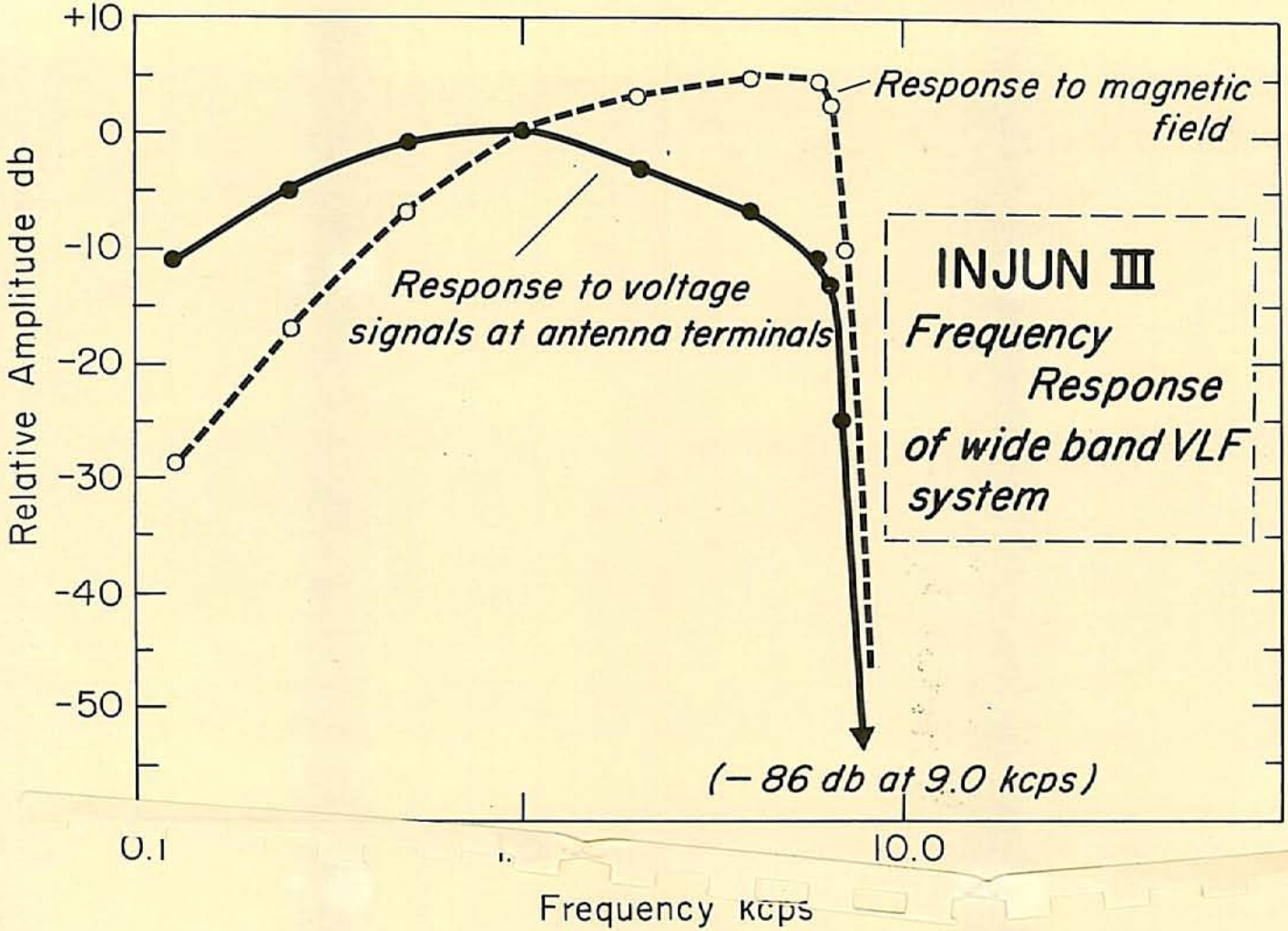
+10
0
-10
-20
-30
-40
-50
Relative Amplitude db
Response to magnetic field
Response to voltage signals at antenna terminals
INJUN III
Frequency Response of wide band VLF system
(– 86 db at 9.0 kcps)
0.1
10.0
Frequency kcps

FIGURE 4

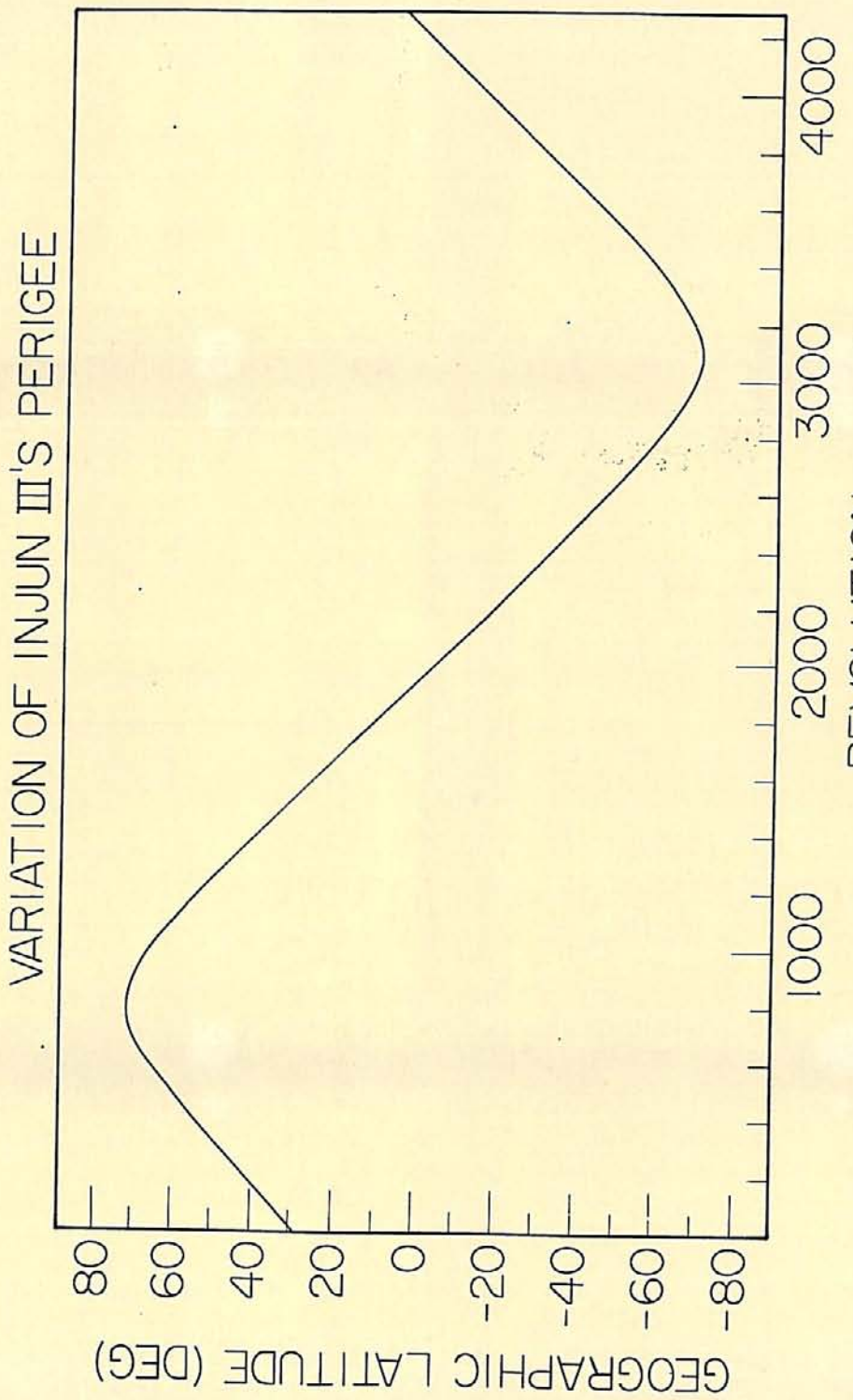
VARIATION OF INJUN III'S PERIGEE
GEOGRAPHIC LATITUDE (DEG)
80
60
40
20
0
-20
-40
-60
-80
1000
2000
3000
4000
REVOLUTION
G67-345

FIGURE 5

G67-376

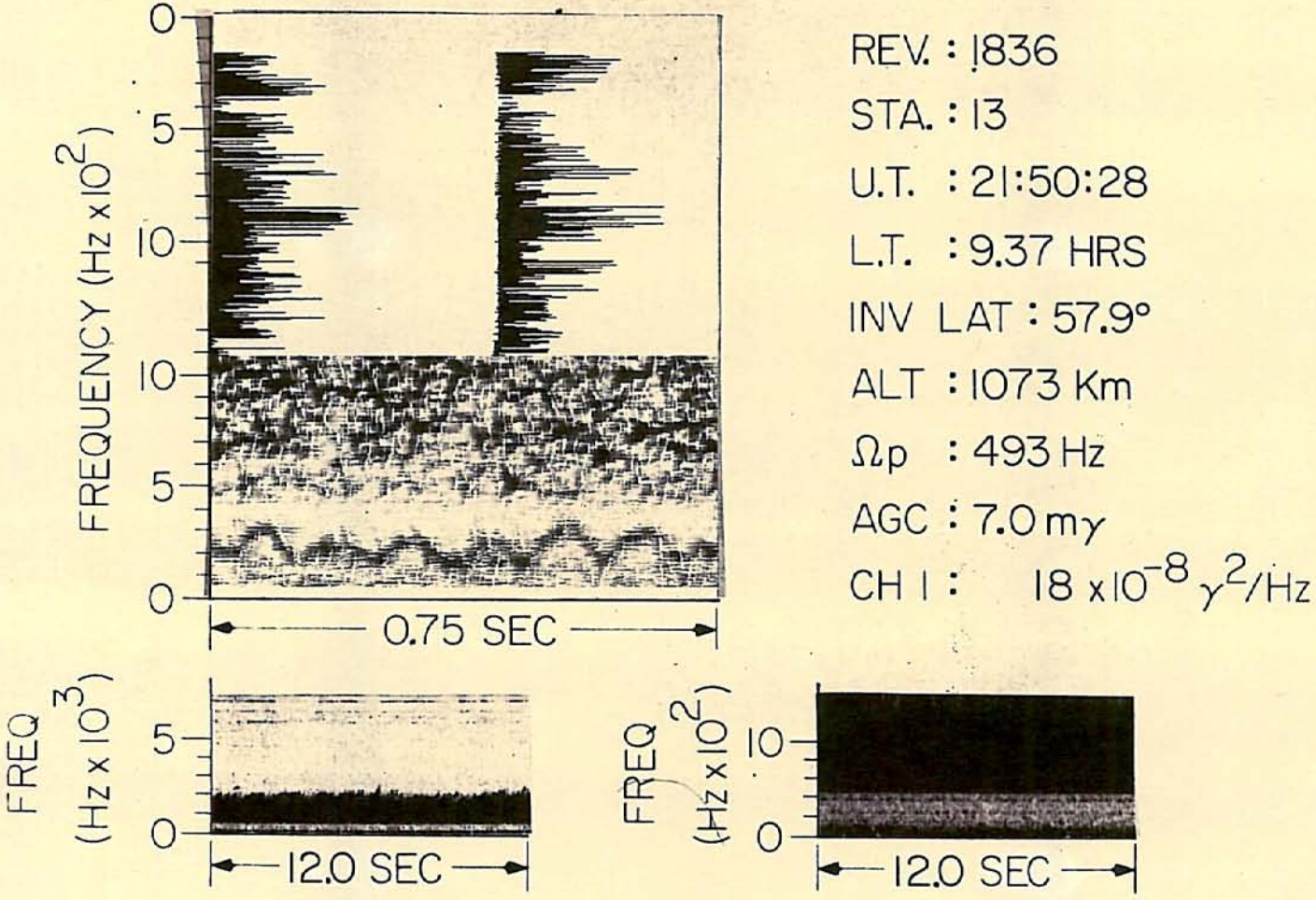

REV. : 1836
STA. : 13
U.T. : 21:50:28
L.T. : 9.37 HRS
INV LAT : 57.9°
ALT : 1073 Km
Ωp : 493 Hz
AGC : 7.0 mγ
CH 1 : $18 \times 10^{-8}\ \gamma^2/Hz$

FIGURE 6

G67-378

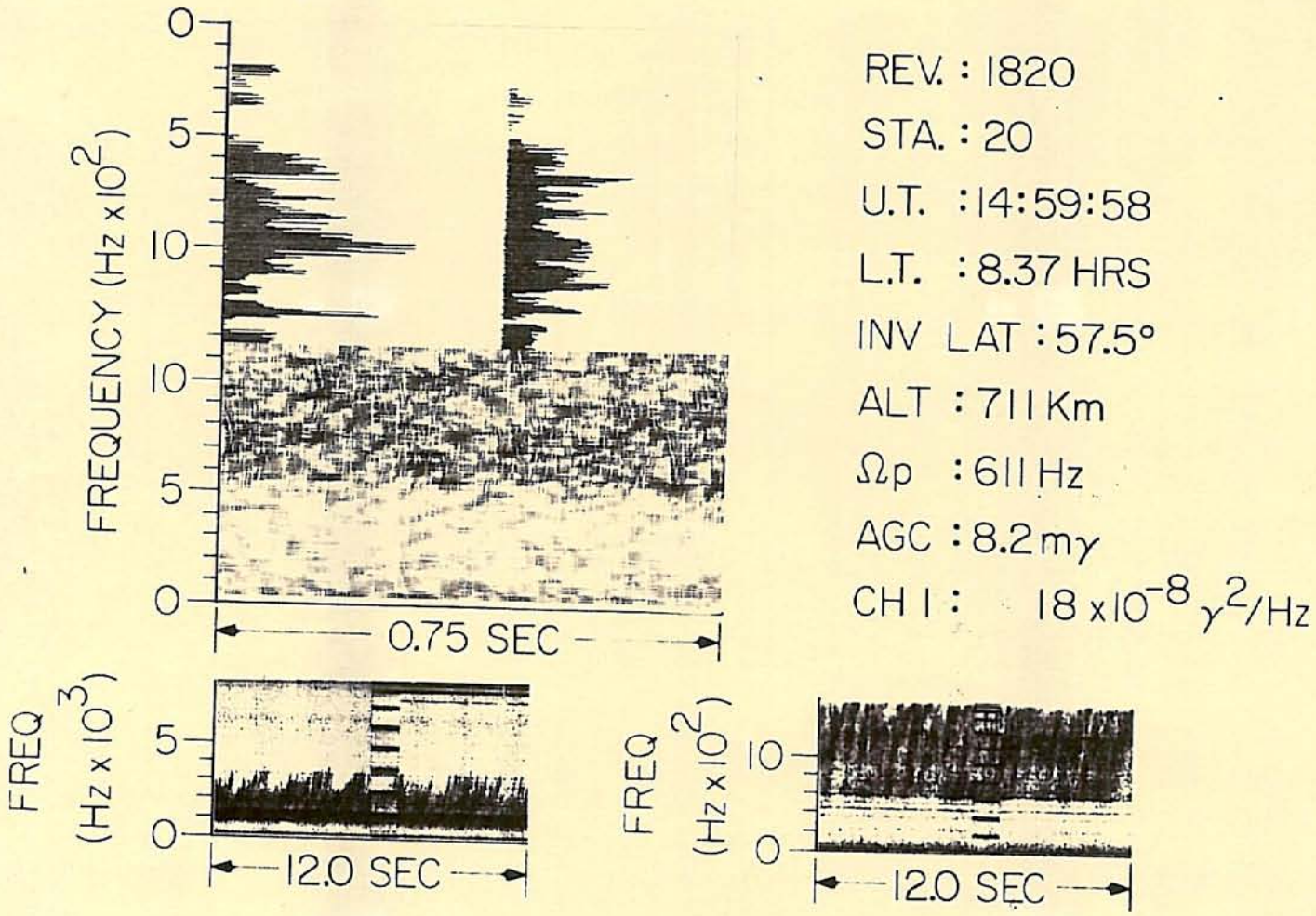

REV. : 1820
STA. : 20
U.T. : 14:59:58
L.T. : 8.37 HRS
INV LAT : 57.5°
ALT : 711 Km
Ωp : 611 Hz
AGC : 8.2 mγ
CH 1 : $18 \times 10^{-8}\ \gamma^2/Hz$

FIGURE 7

G67-374

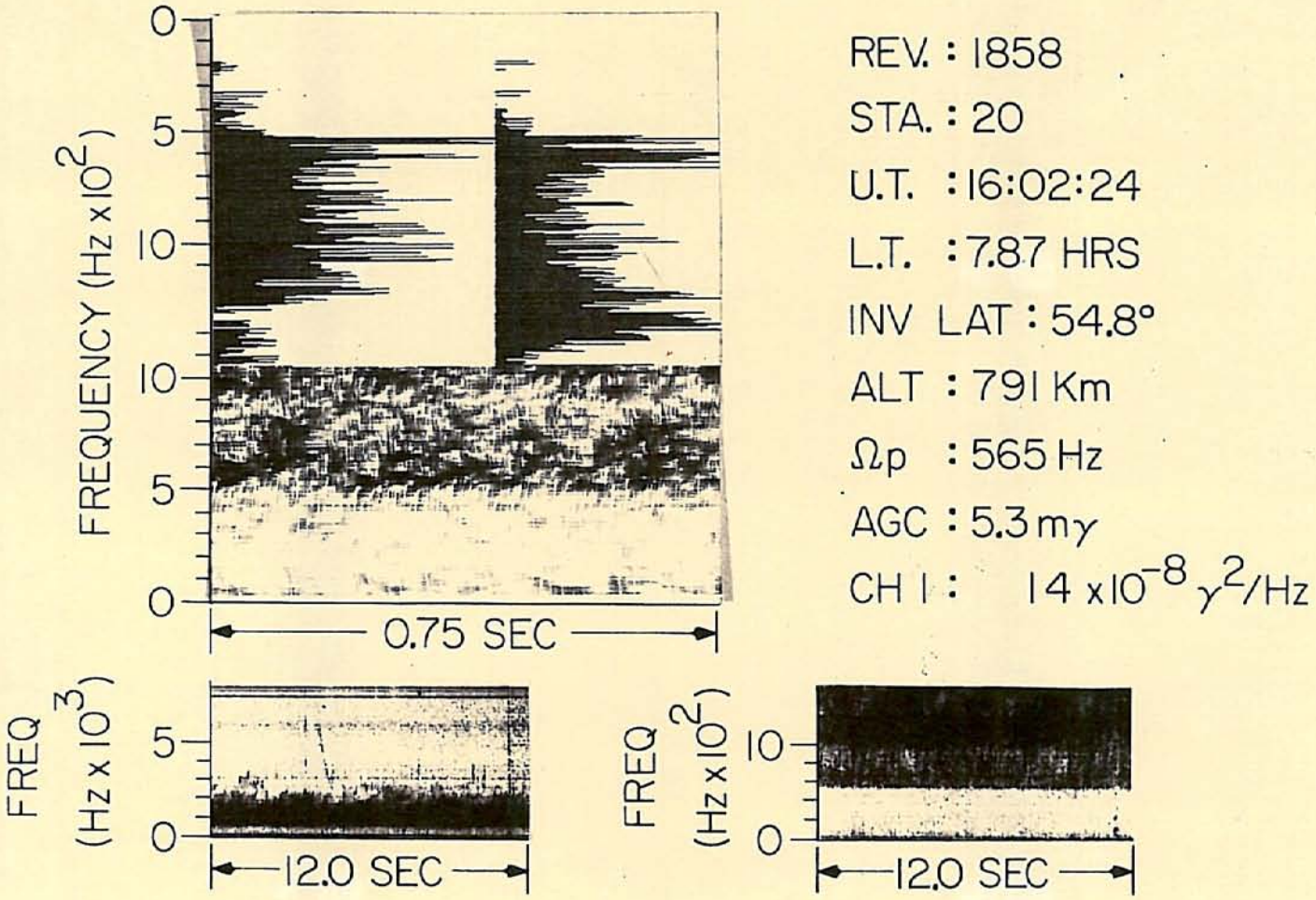

FIGURE 8

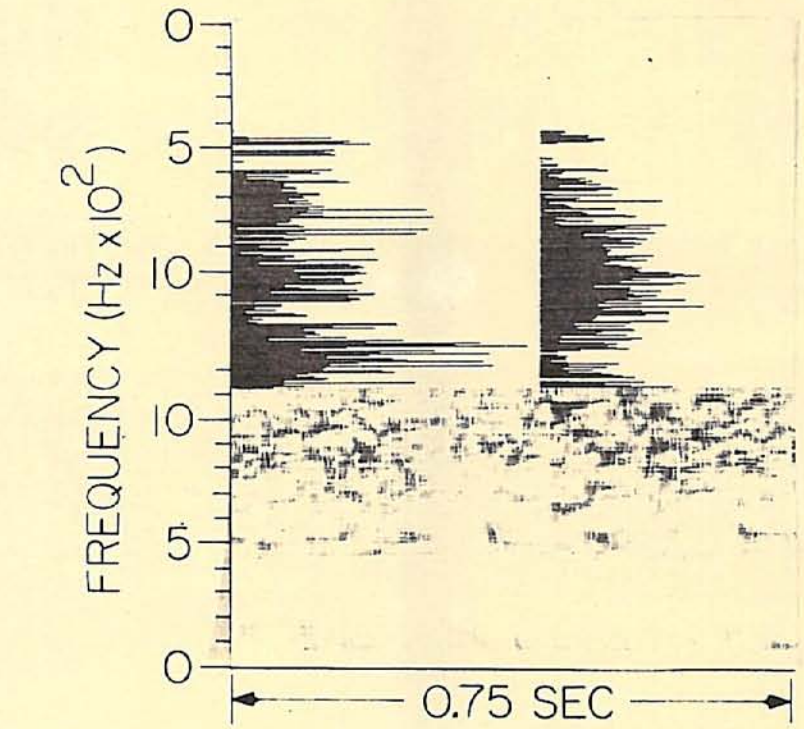

REV. : 1861
STA. : 13
U.T. : 21:54:06
L.T. : 9.33 HRS
INV LAT : 59.7°
ALT : 1173 Km
Ωp : 480 Hz
AGC : 3.5 mγ
CH 1 : $10 \times 10^{-8}\ \gamma^2/Hz$

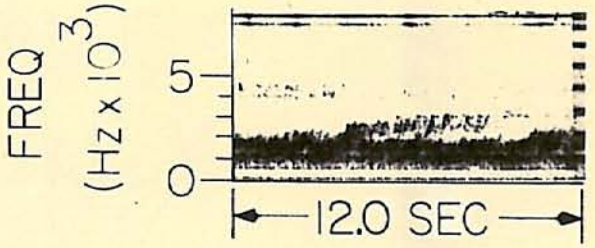

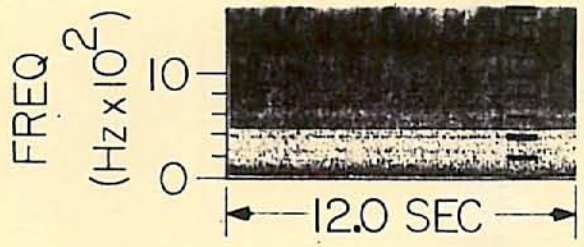

FIGURE 9

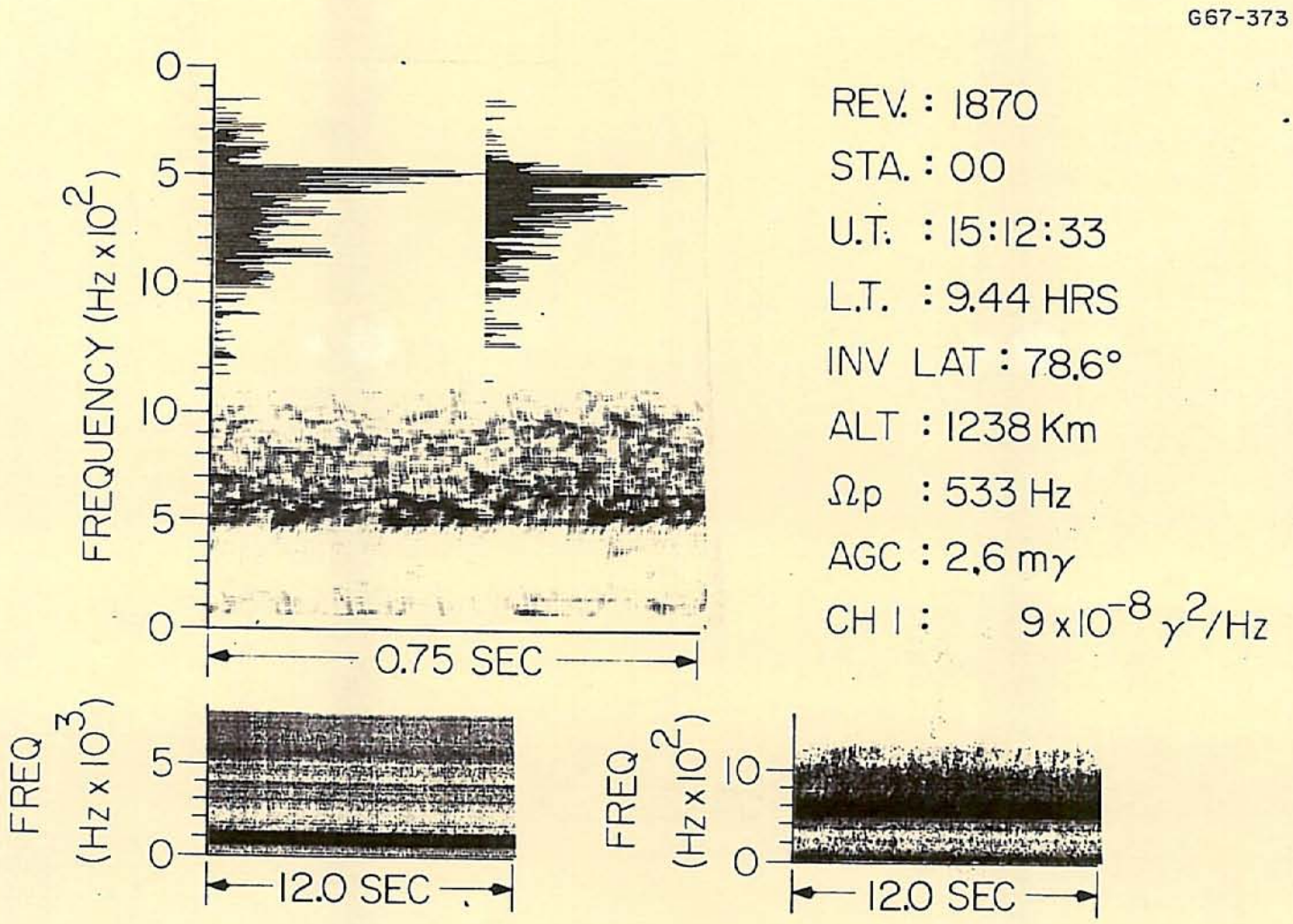
G67-373
FREQUENCY (Hz x 10^2)
0
5
10
10
5
0
0.75 SEC
REV. : 1870
STA. : 00
U.T. : 15:12:33
L.T. : 9.44 HRS
INV LAT : 78.6°
ALT : 1238 Km
Ωp : 533 Hz
AGC : 2.6 mγ
CH 1 : 9 x 10^-8 γ^2/Hz
FREQ (Hz x 10^3)
5
0
12.0 SEC
FREQ (Hz x 10^2)
10
0
12.0 SEC

FIGURE 10

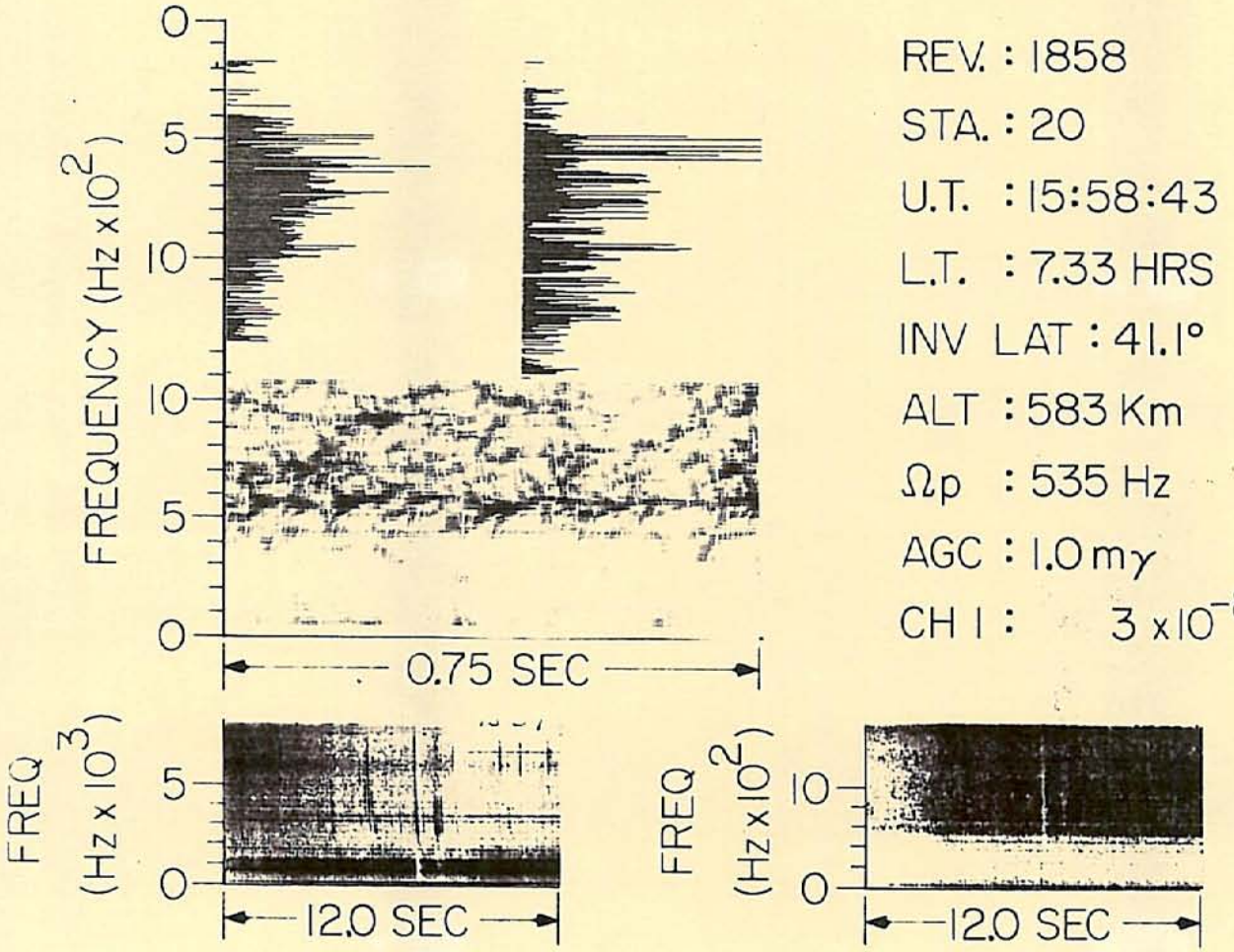

REV. : 1858
STA. : 20
U.T. : 15:58:43
L.T. : 7.33 HRS
INV LAT : 41.1°
ALT : 583 Km
Ωp : 535 Hz
AGC : 1.0 mγ
CH 1 : $3 \times 10^{-8}\ \gamma^2/Hz$

FIGURE 11

G67-377

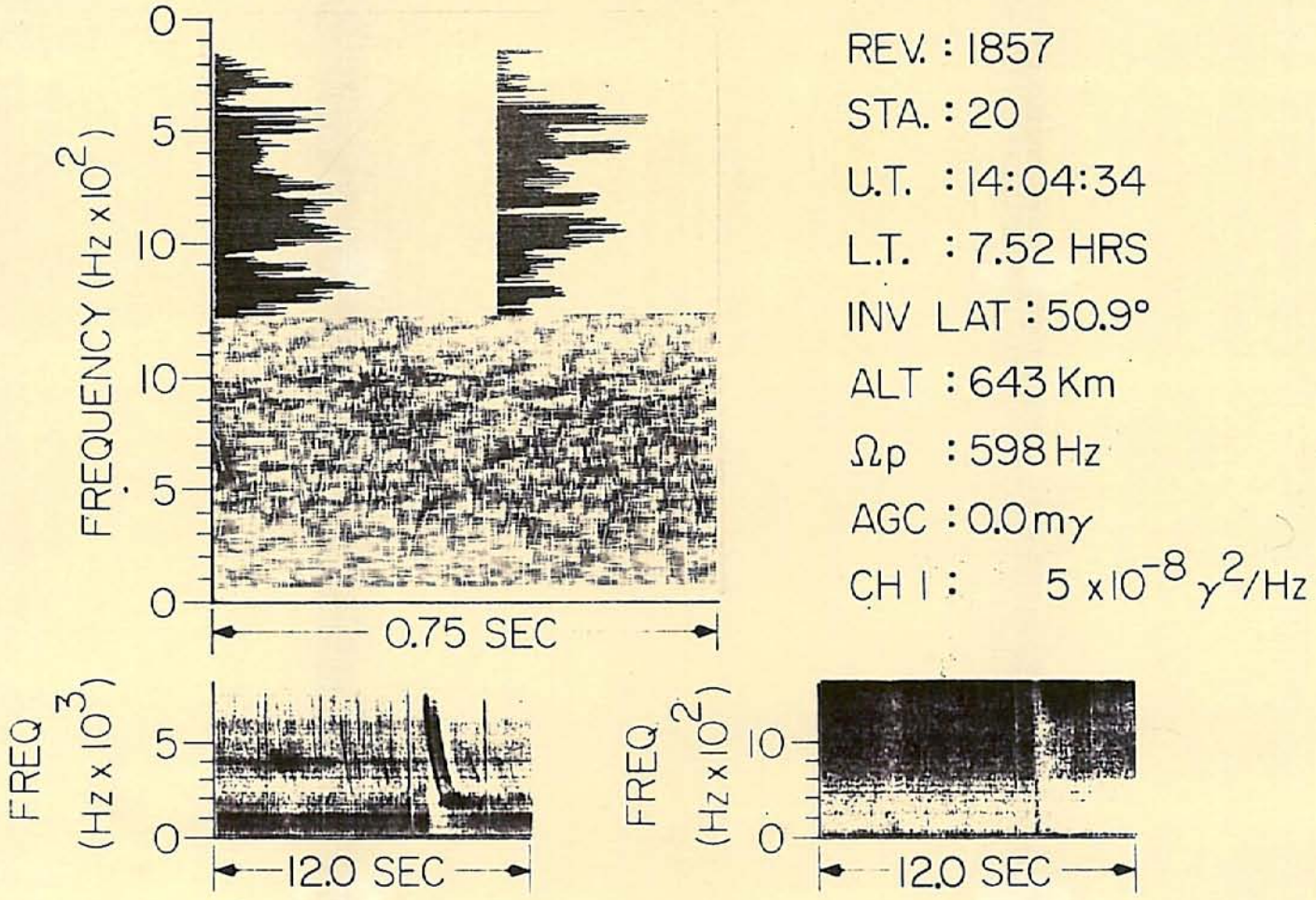

REV. : 1857
STA. : 20
U.T. : 14:04:34
L.T. : 7.52 HRS
INV LAT : 50.9°
ALT : 643 Km
Ωp : 598 Hz
AGC : 0.0 mγ
CH 1 : $5 \times 10^{-8}\ \gamma^2/Hz$

09

FIGURE 12

G67-426

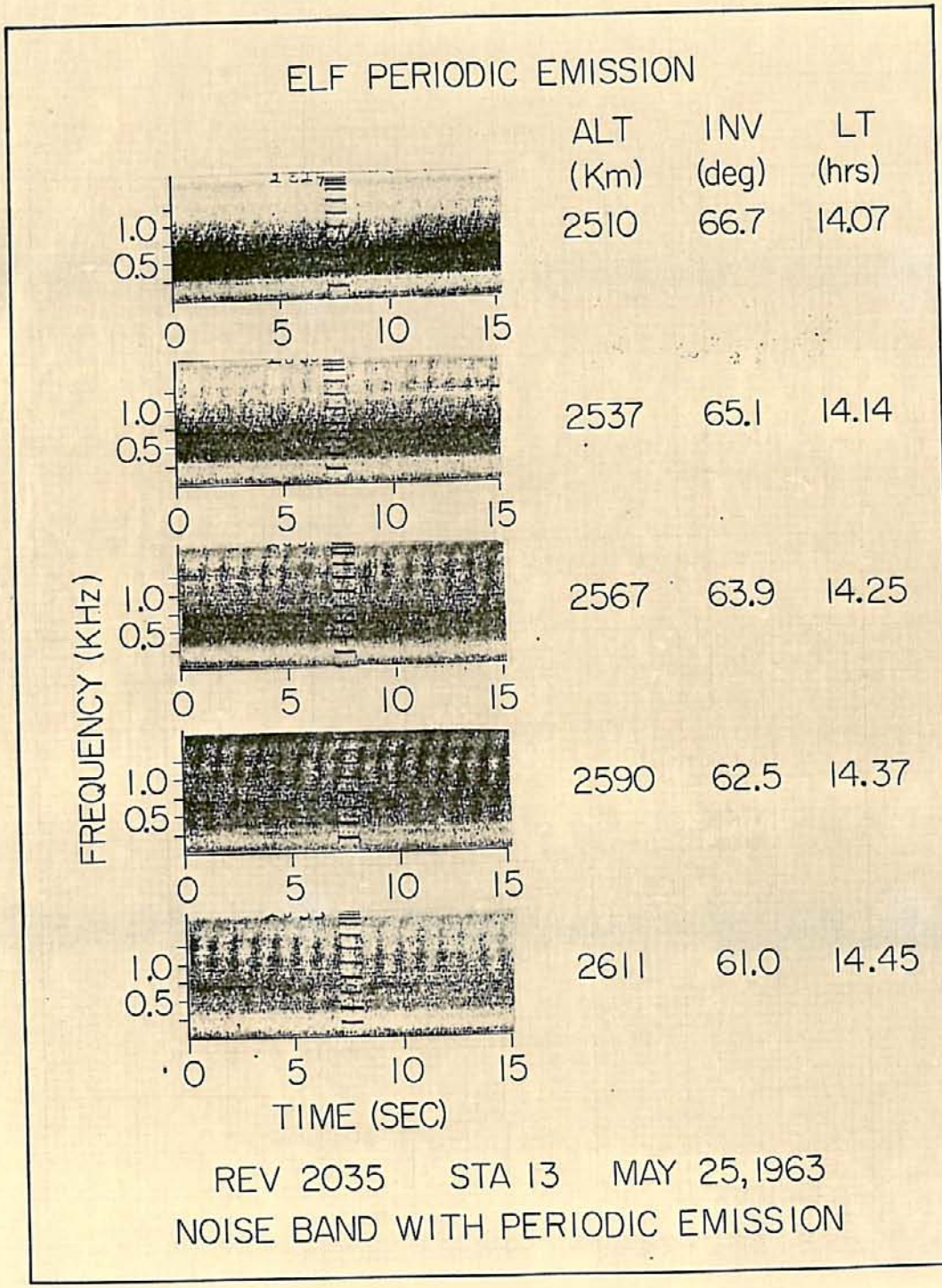

FIGURE 13

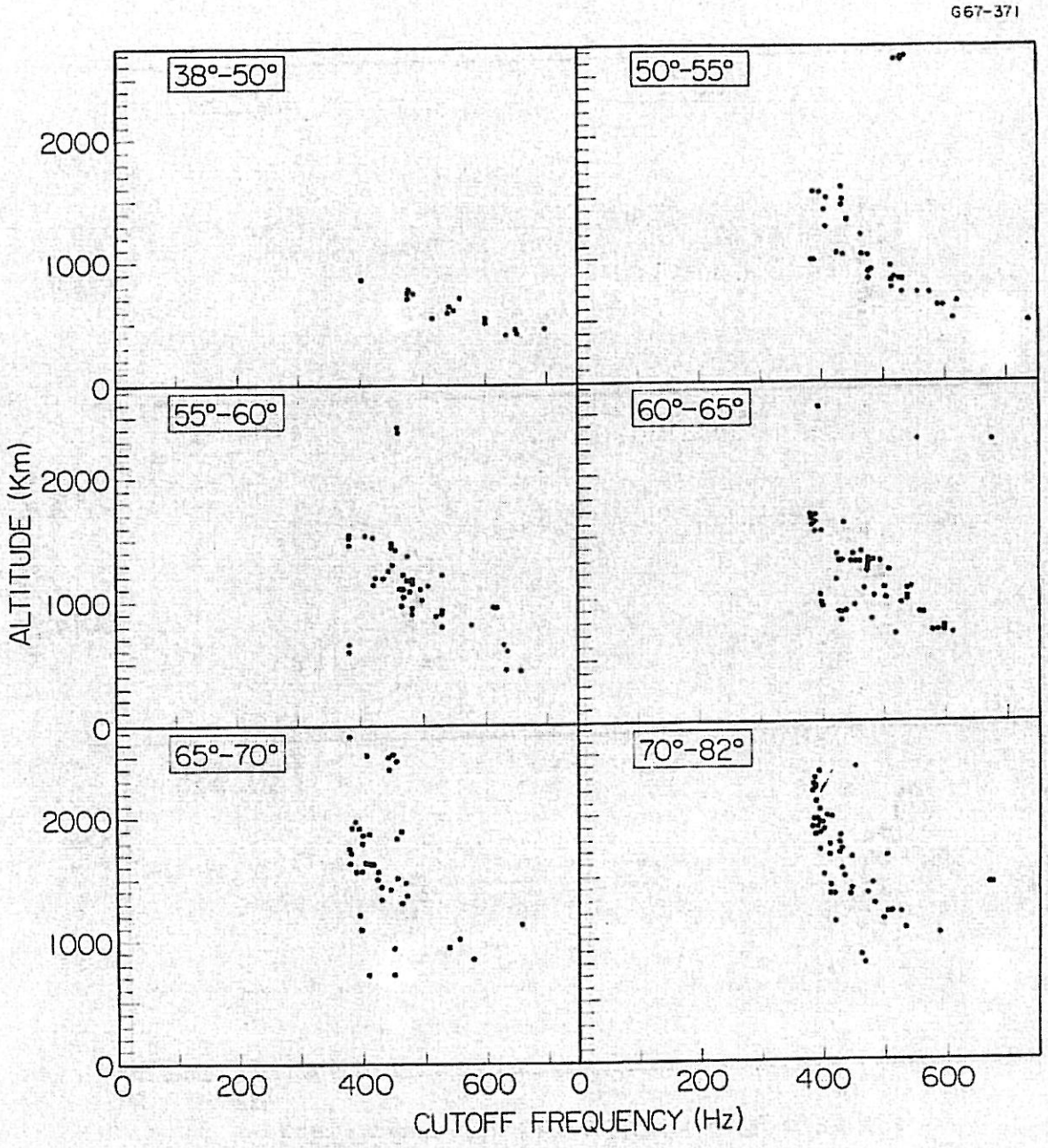
G67-371
38°-50°
50°-55°
55°-60°
60°-65°
65°-70°
70°-82°
ALTITUDE (Km)
2000
1000
0
0
200
400
600
CUTOFF FREQUENCY (Hz)

Figure 14

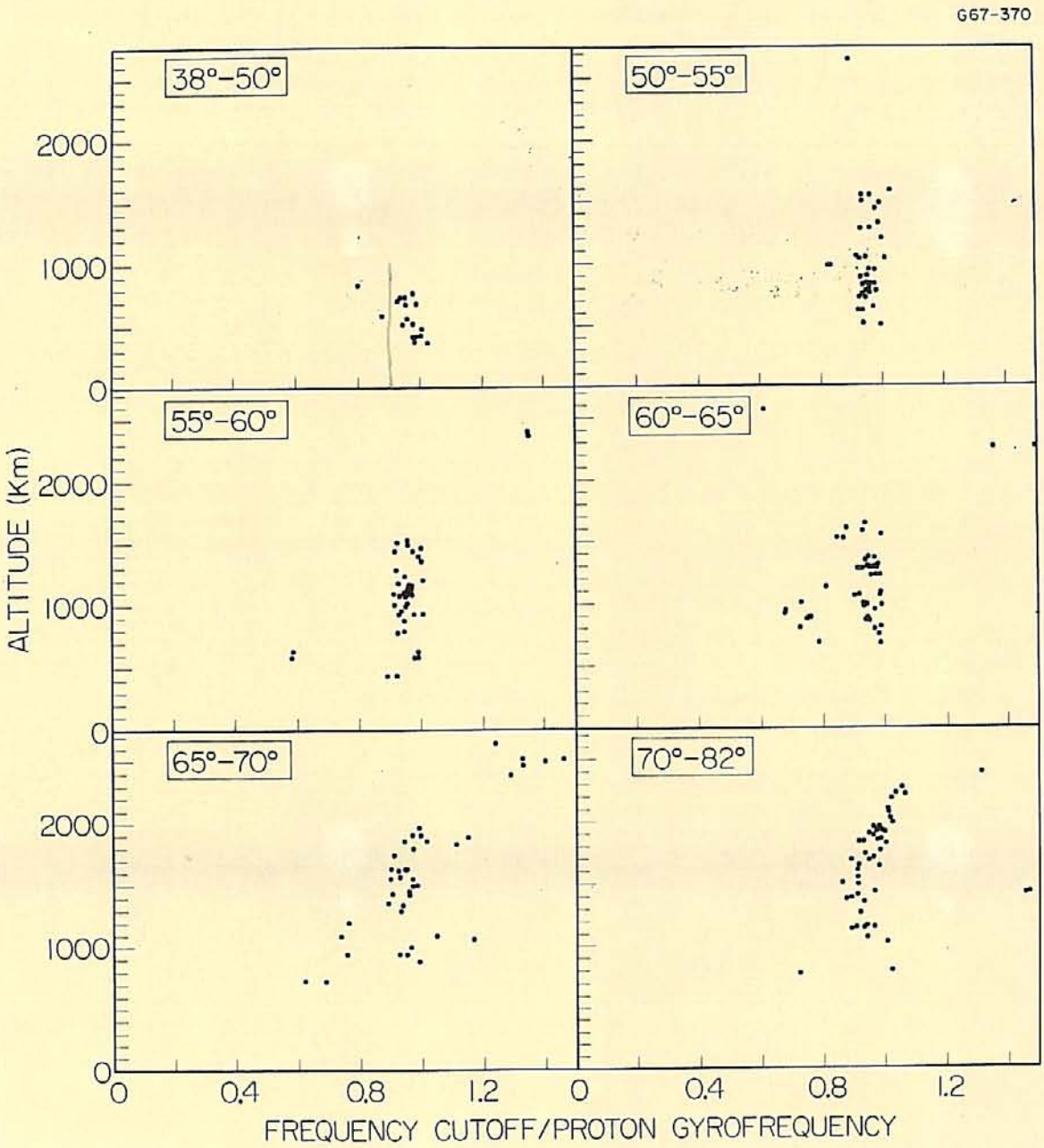
G67-370
38°–50°
50°–55°
55°–60°
60°–65°
65°–70°
70°–82°
ALTITUDE (Km)
2000
1000
0
0
0.4
0.8
1.2
FREQUENCY CUTOFF/PROTON GYROFREQUENCY

FIGURE 15

G67-436

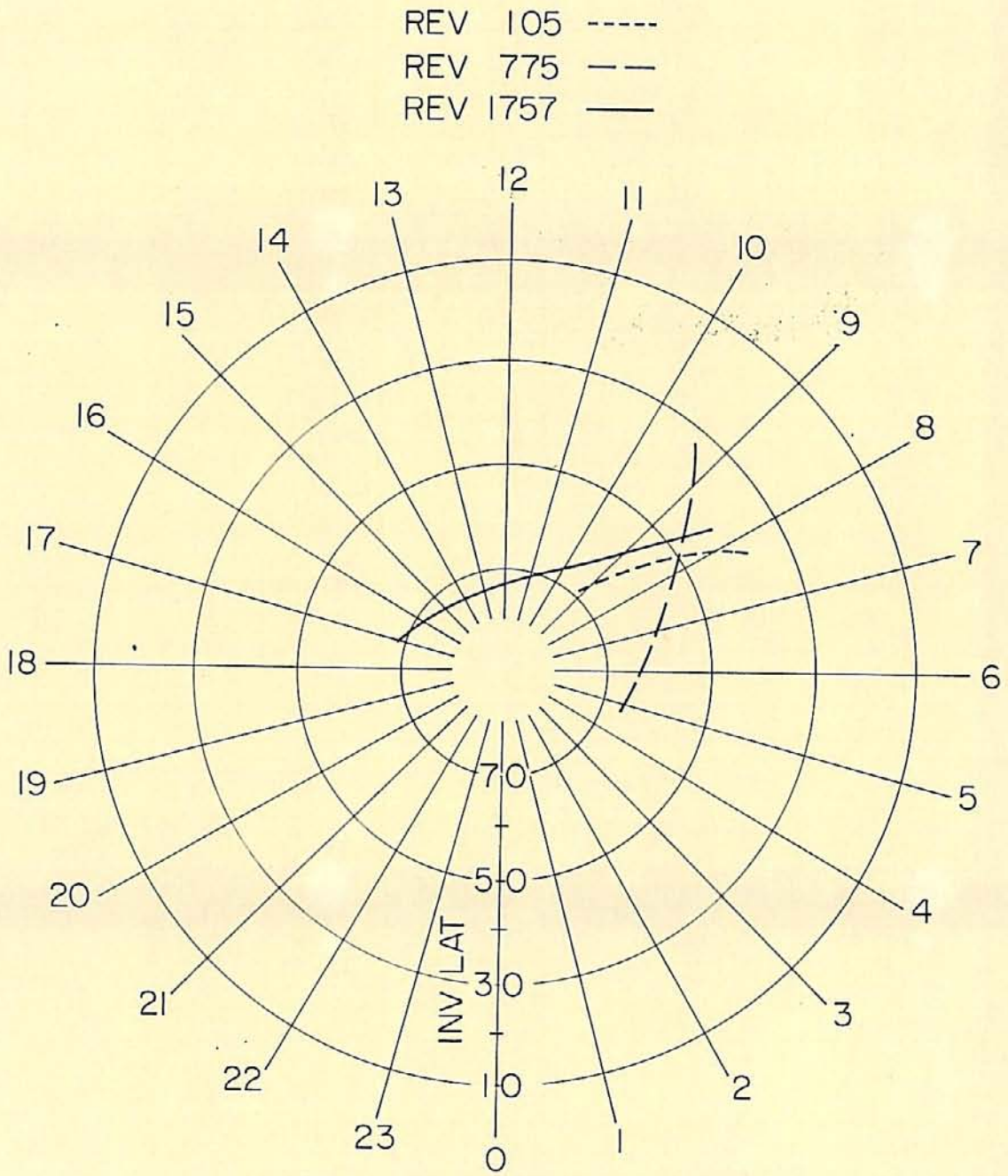

FIGURE 16

G67-366

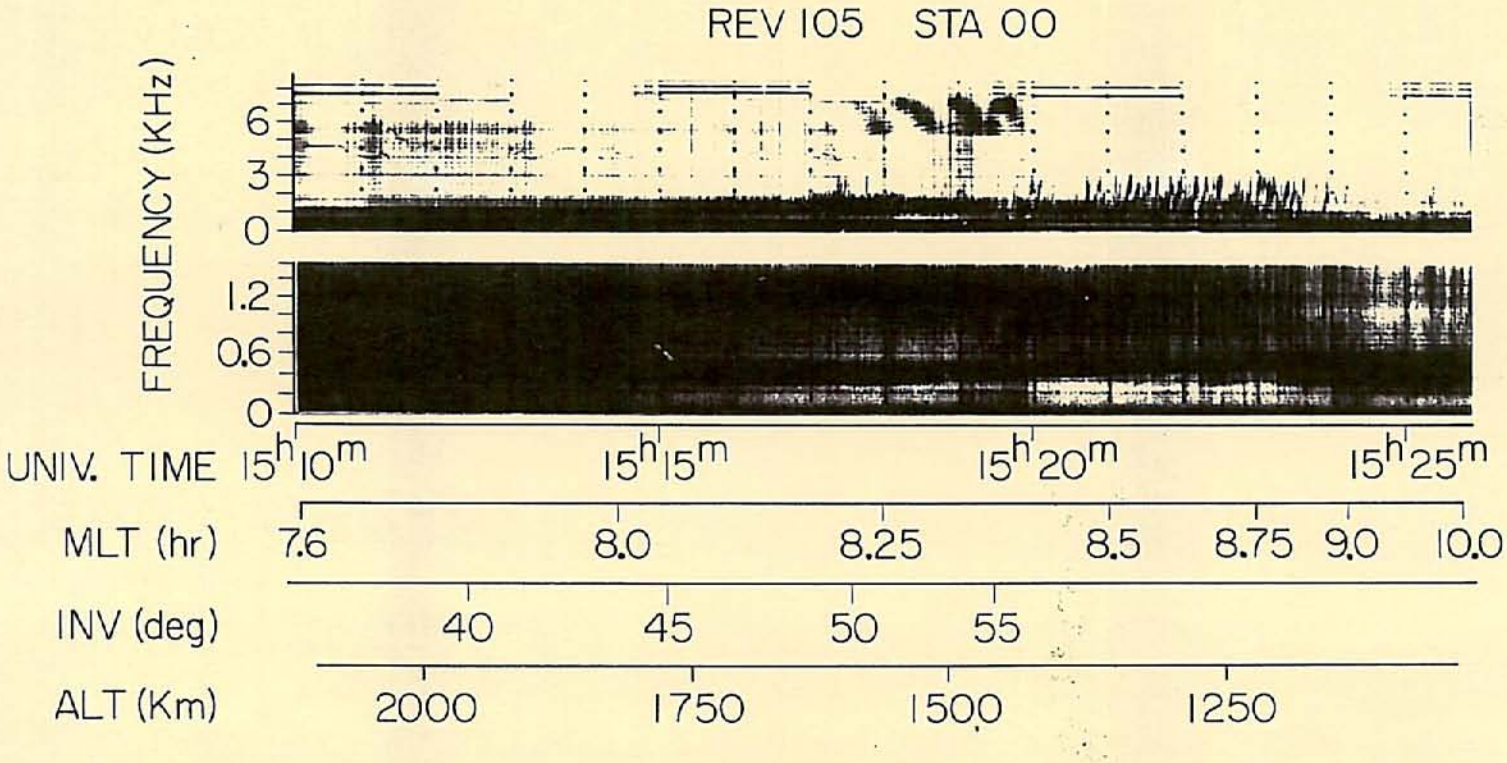

FIGURE 17

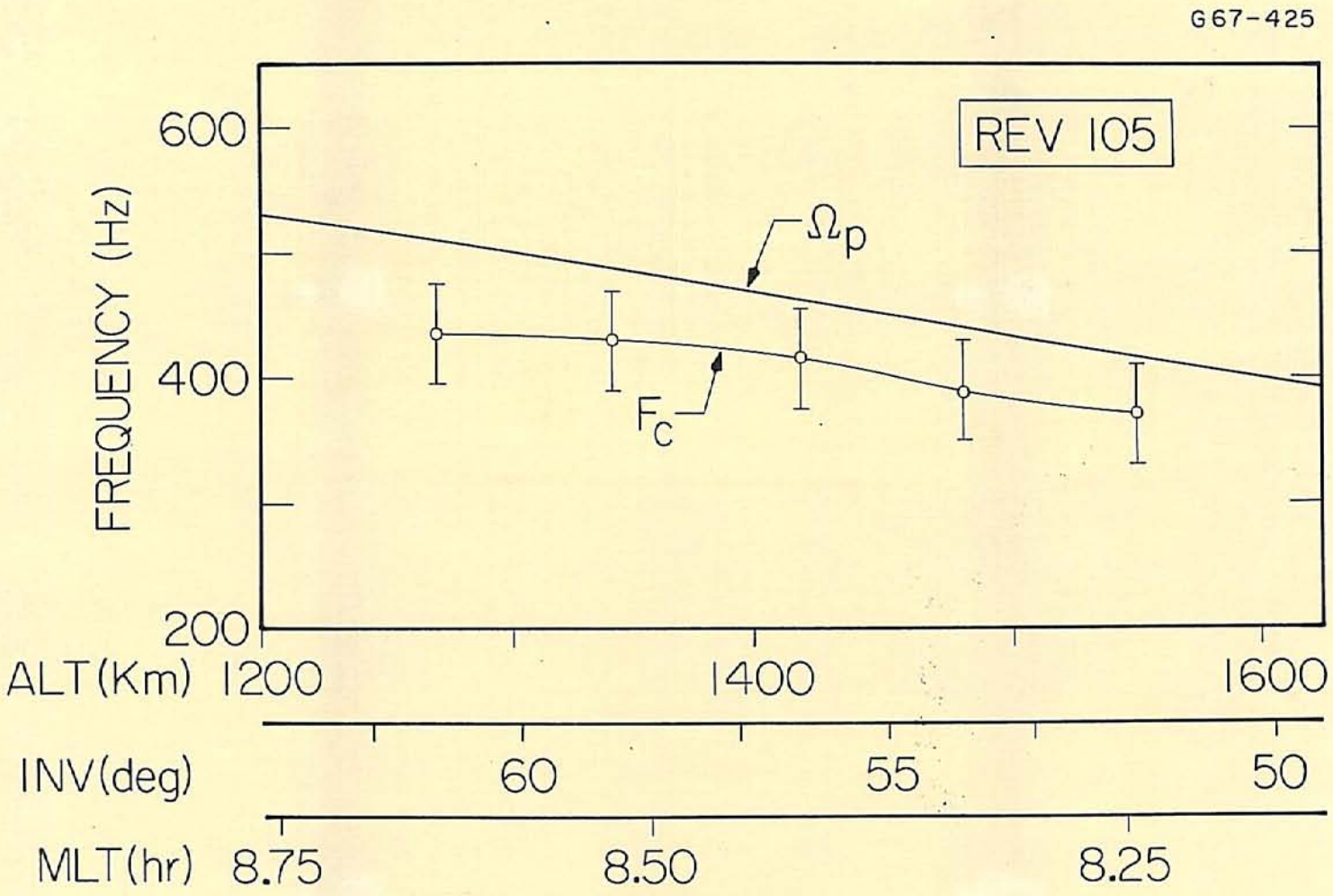
G67-425
REV 105
FREQUENCY (Hz)
600
400
200
Ω_p
F_C
ALT(Km) 1200
1400
1600
INV(deg)
60
55
50
MLT(hr) 8.75
8.50
8.25

FIGURE 18

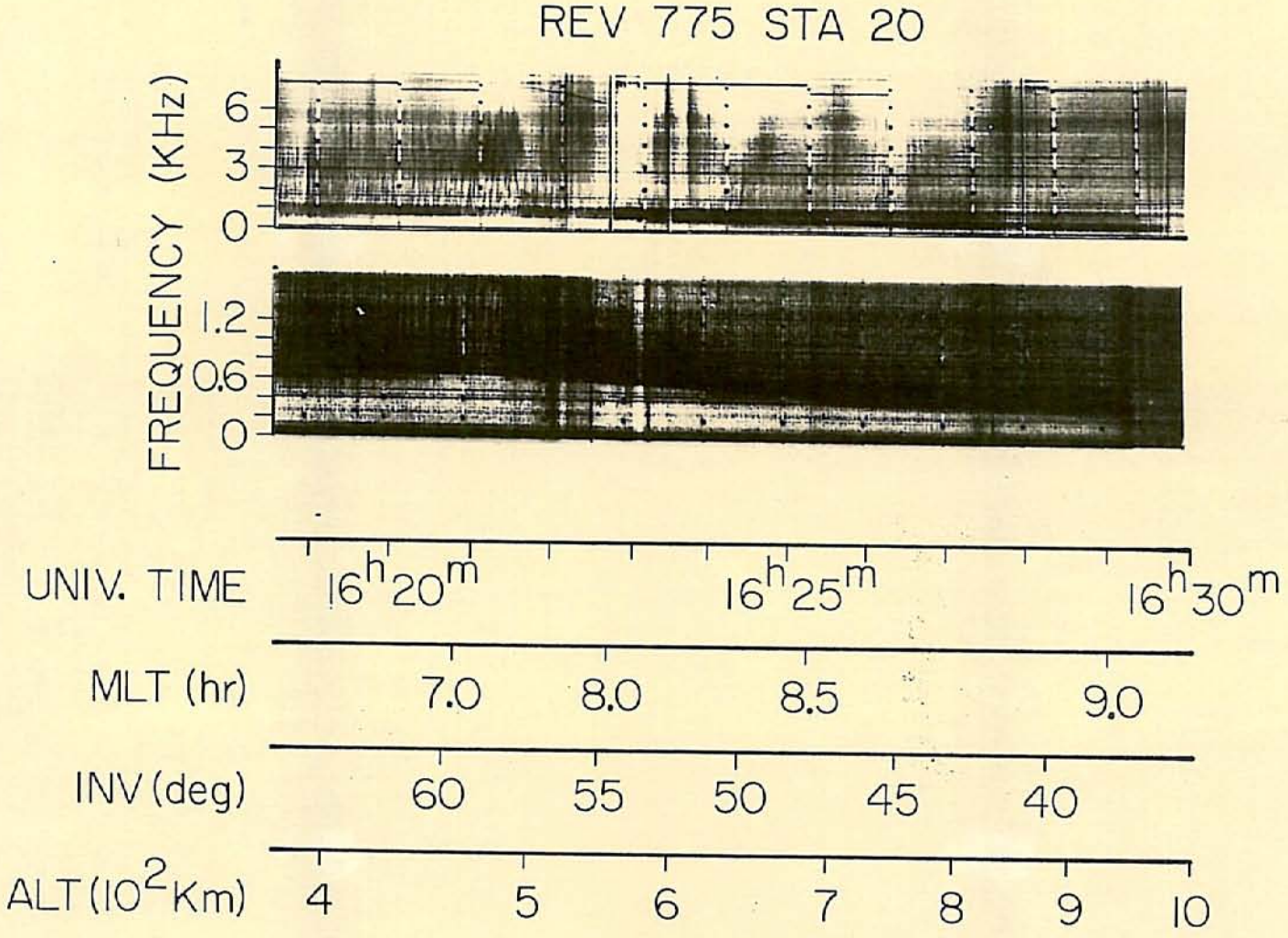
REV 775 STA 20
FREQUENCY (KHz)
6
3
0
1.2
0.6
0
UNIV. TIME
16h20m
16h25m
16h30m
MLT (hr)
7.0
8.0
8.5
9.0
INV (deg)
60
55
50
45
40
ALT (10²Km)
4
5
6
7
8
9
10

FIGURE 19

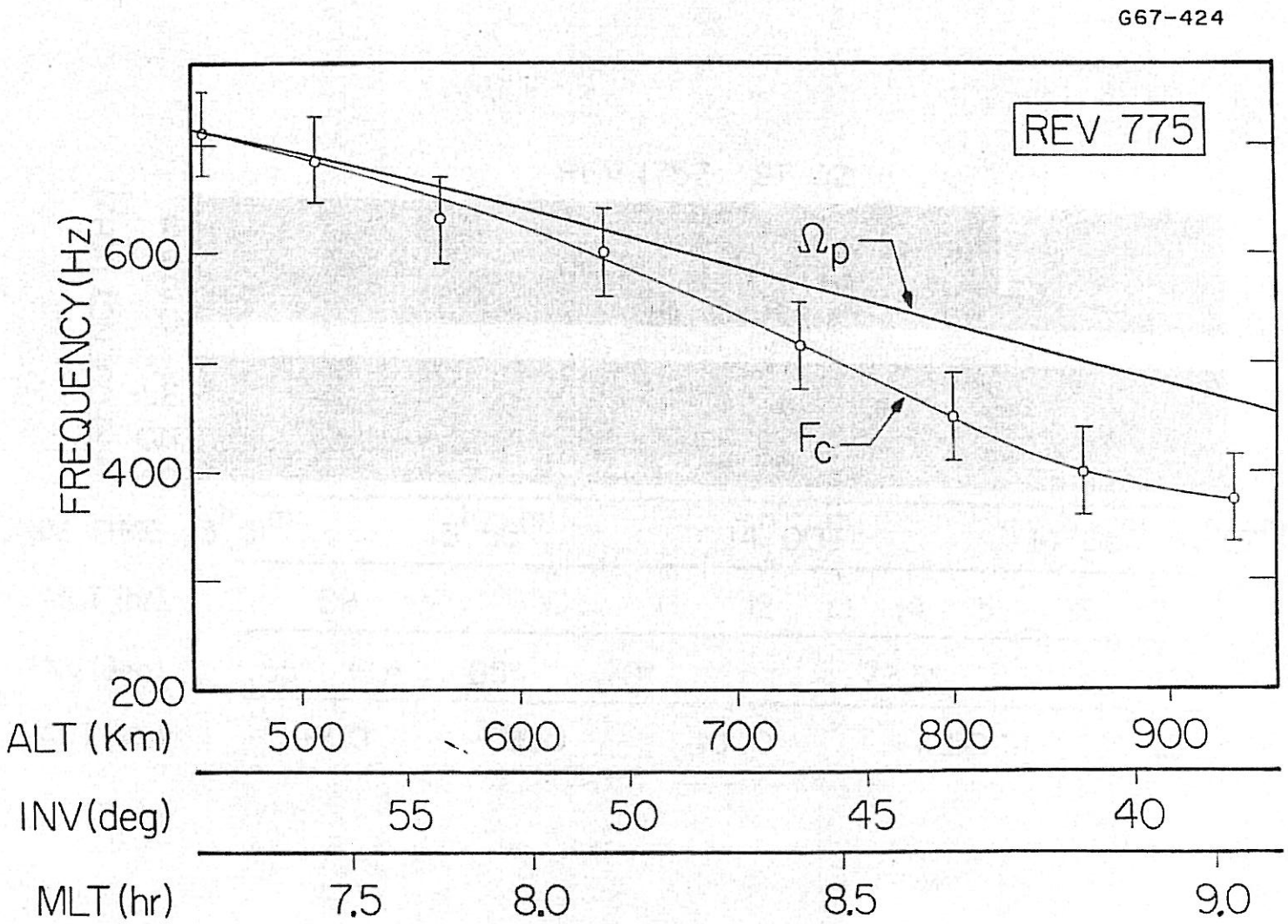
G67-424
REV 775
Ω_p
F_c
FREQUENCY (Hz)
600
400
200
ALT (Km)
500
600
700
800
900
INV (deg)
55
50
45
40
MLT (hr)
7.5
8.0
8.5
9.0

Figure 20

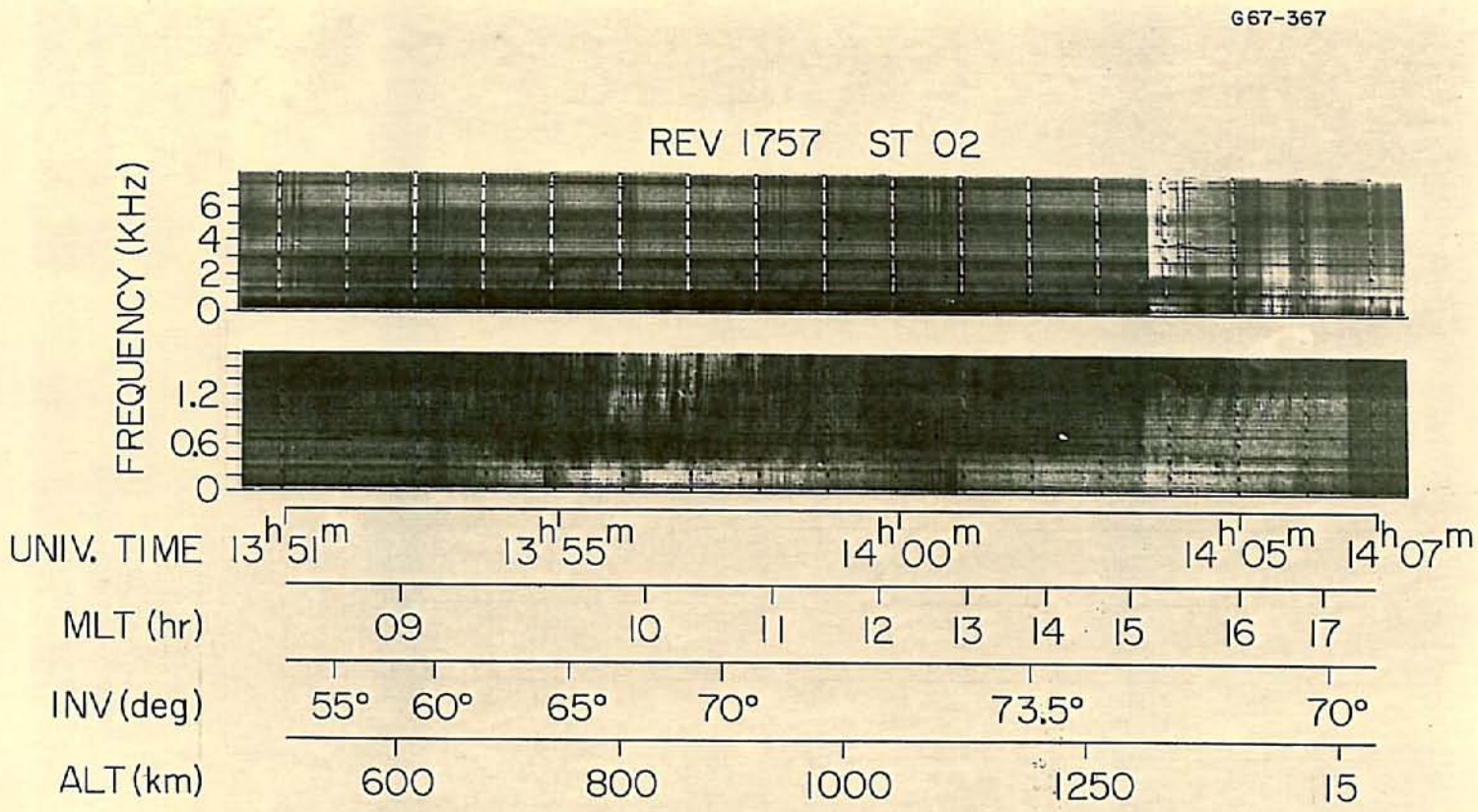
G67-367
REV 1757 ST 02
FREQUENCY (KHz)
6
4
2
0
1.2
0.6
0
UNIV. TIME 13h51m 13h55m 14h00m 14h05m 14h07m
MLT (hr) 09 10 11 12 13 14 15 16 17
INV (deg) 55° 60° 65° 70° 73.5° 70°
ALT (km) 600 800 1000 1250 15

FIGURE 21

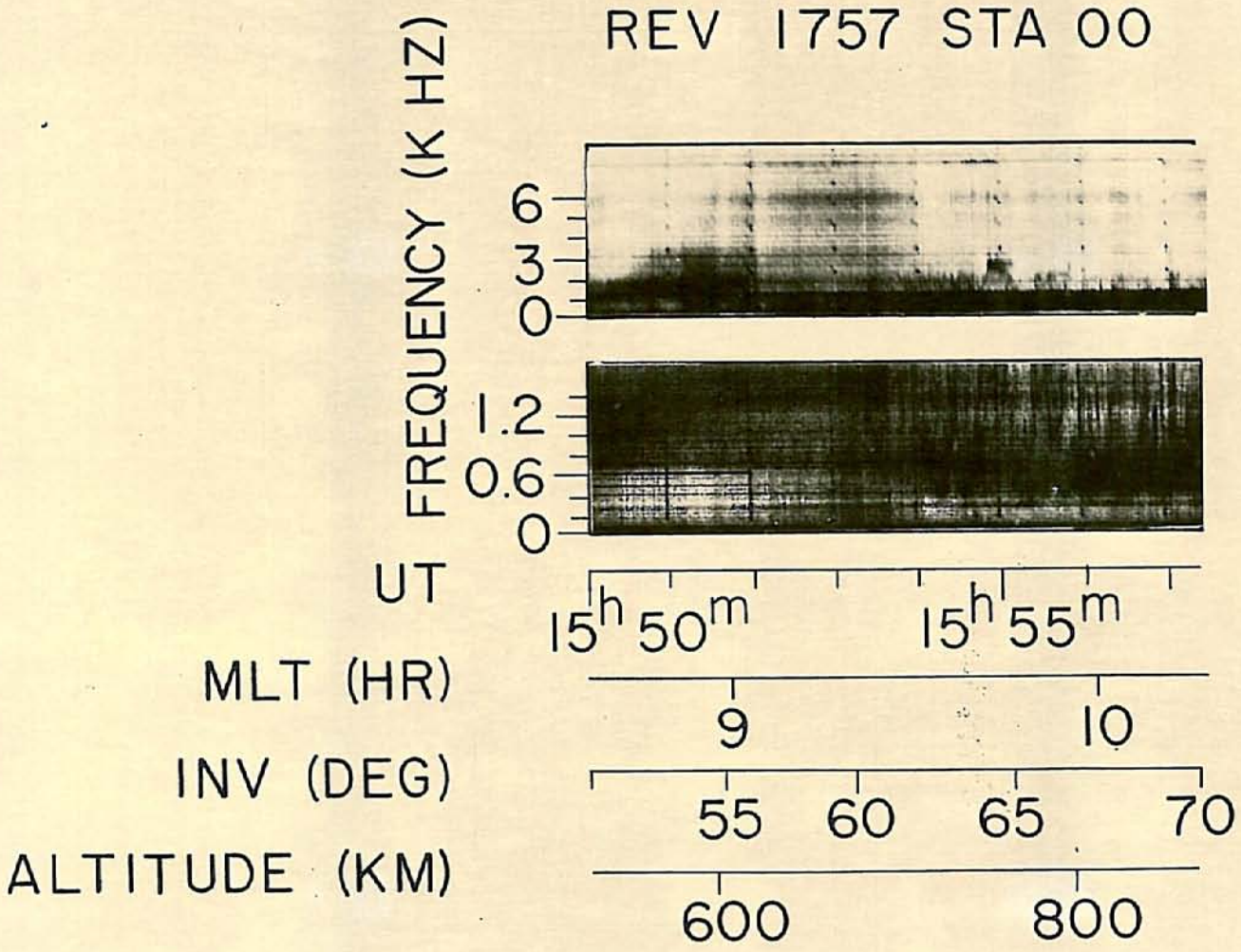
REV 1757 STA 00
FREQUENCY (K HZ)
6
3
0
1.2
0.6
0
UT
15h 50m
15h 55m
MLT (HR)
9
10
INV (DEG)
55
60
65
70
ALTITUDE (KM)
600
800

FIGURE 22

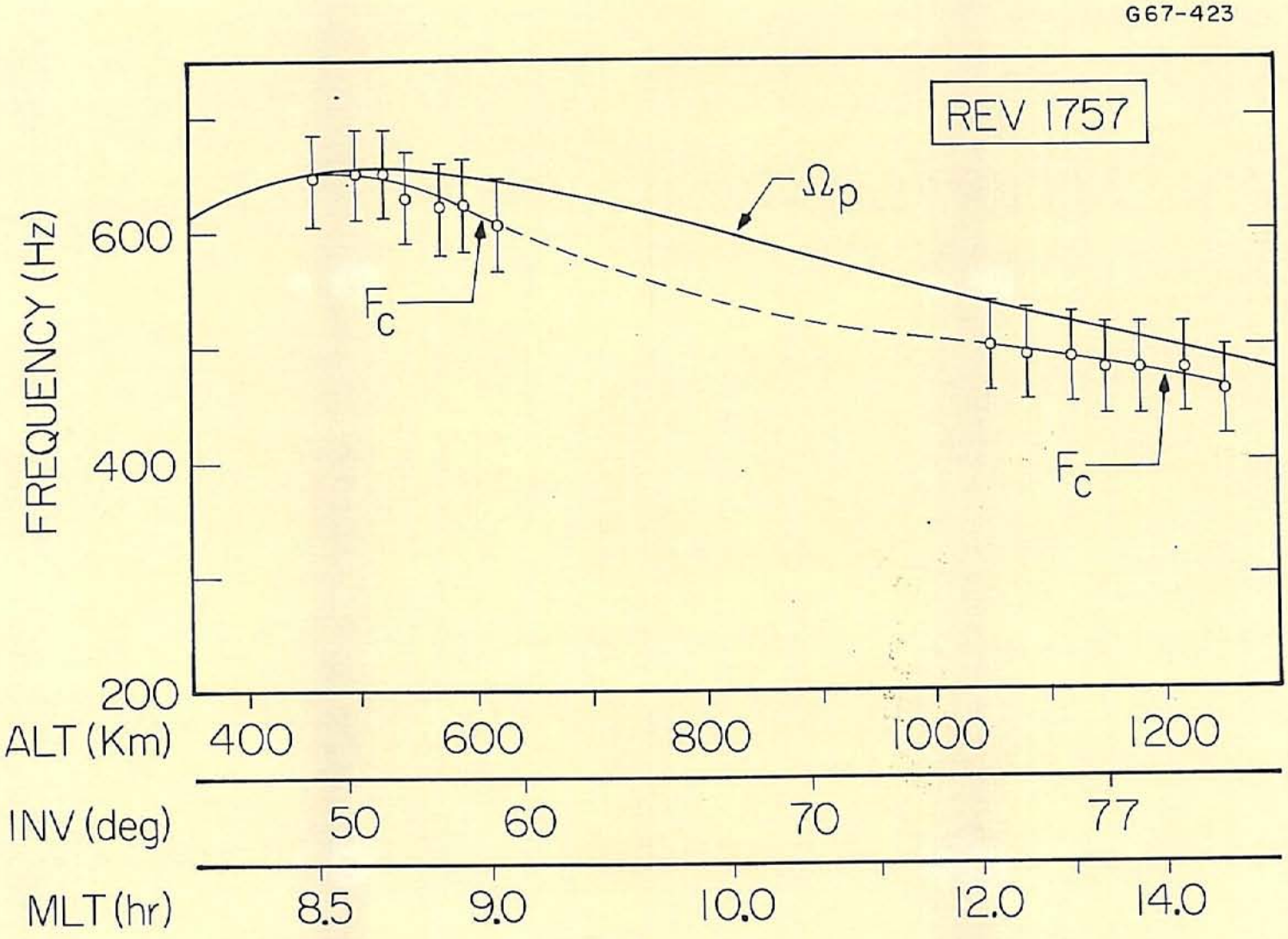
G67-423
REV 1757
Ω_p
F_c
F_c
FREQUENCY (Hz)
600
400
200
ALT (Km)
400
600
800
1000
1200
INV (deg)
50
60
70
77
MLT (hr)
8.5
9.0
10.0
12.0
14.0

FIGURE 23

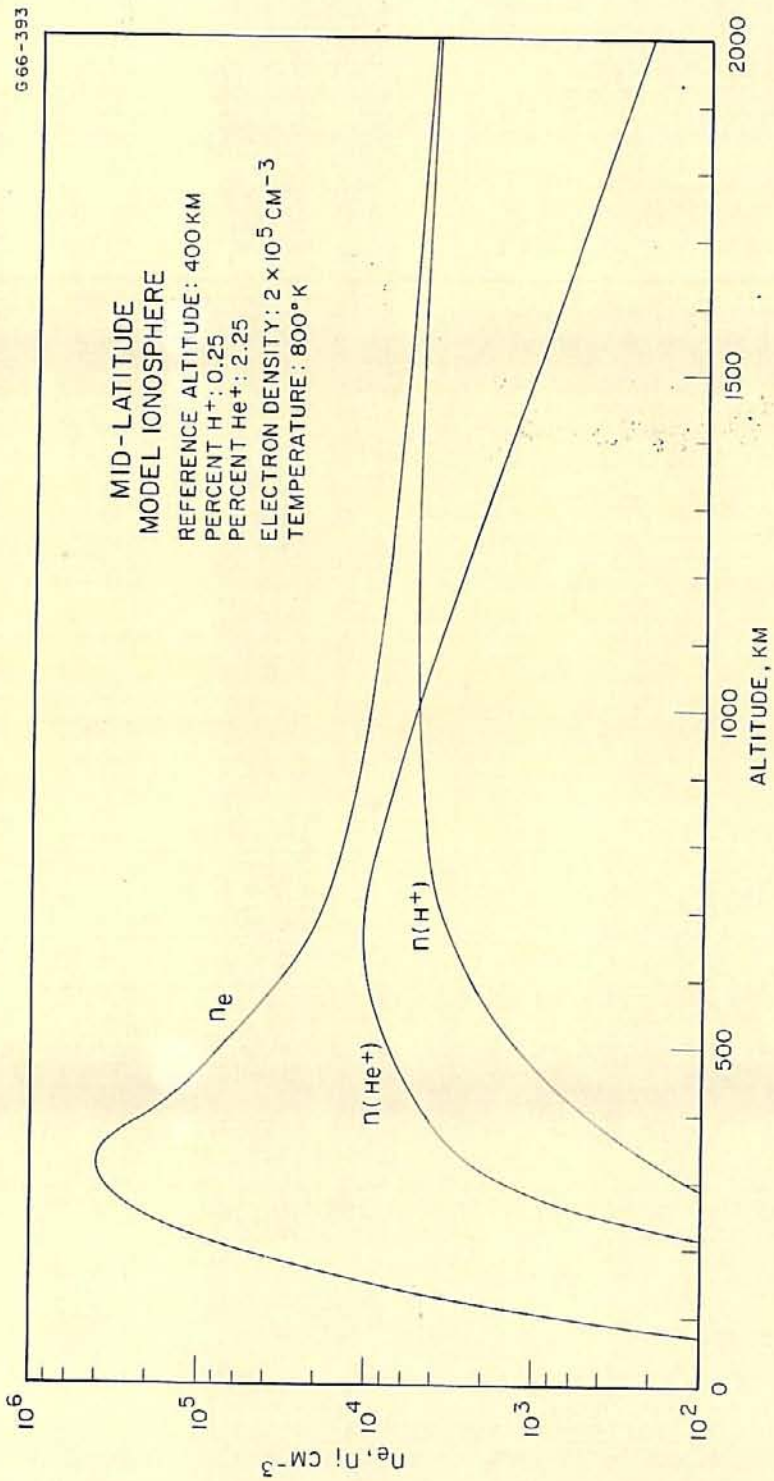
G66-393
MID-LATITUDE
MODEL IONOSPHERE
REFERENCE ALTITUDE: 400 KM
PERCENT H+: 0.25
PERCENT He+: 2.25
ELECTRON DENSITY: 2 x 10^5 CM^-3
TEMPERATURE: 800°K
ne
n(He+)
n(H+)
ne, ni CM-3
ALTITUDE, KM
0
500
1000
1500
2000

FIGURE 24

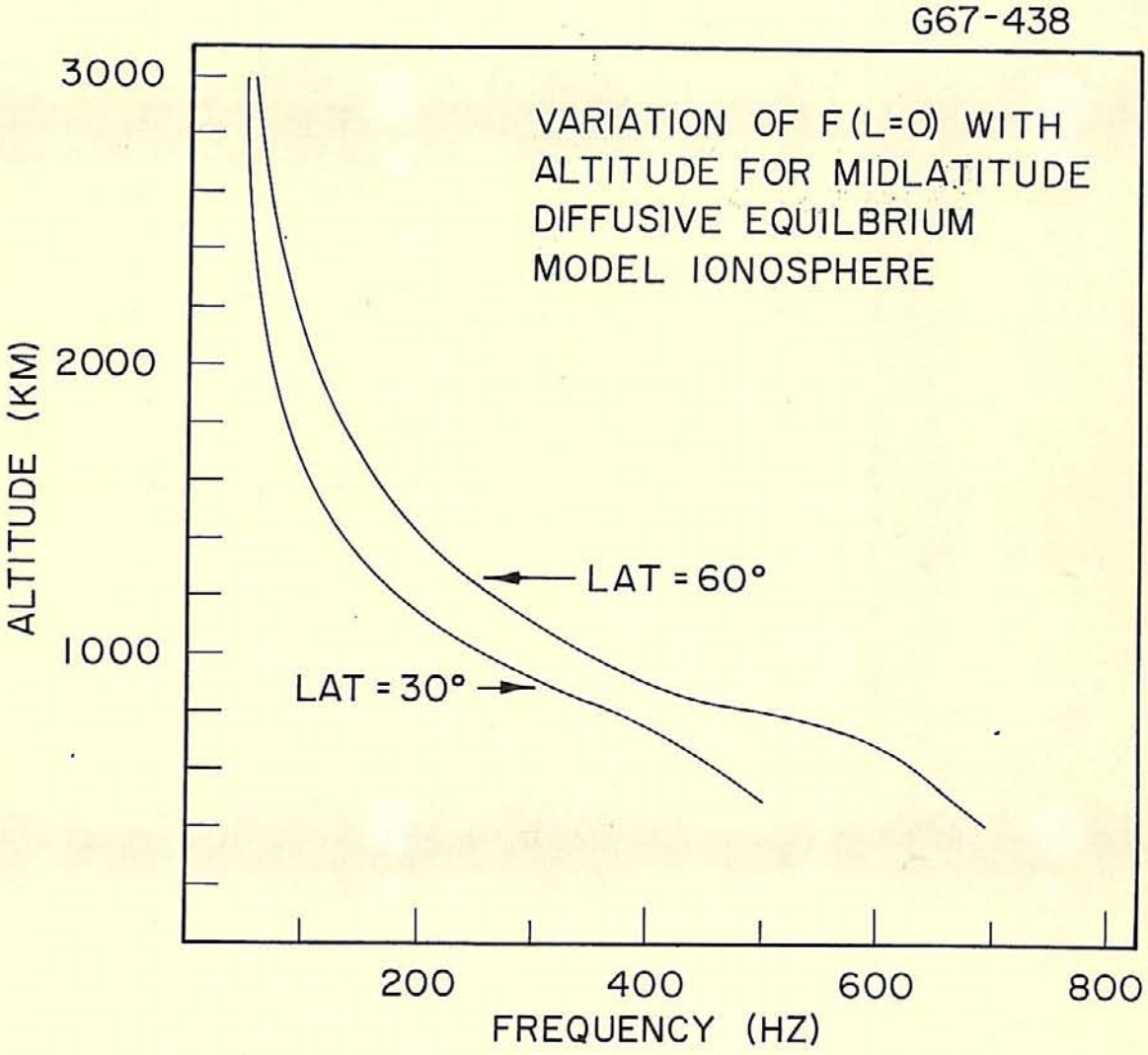
G67-438
VARIATION OF F(L=0) WITH ALTITUDE FOR MIDLATITUDE DIFFUSIVE EQUILBRIUM MODEL IONOSPHERE
LAT = 60°
LAT = 30°
ALTITUDE (KM)
3000
2000
1000
200
400
600
800
FREQUENCY (HZ)

FIGURE 25